JACS
JOURNAL OF THE AMERICAN CHEMICAL SOCIETY
Article
Cite This: J. Am. Chem. Soc. 2018, 140, 3892−3906
pubs.acs.org/JACS

Functionally Active Membrane Proteins Incorporated in Mesostructured Silica Films

Justin P. Jahnke,[†] Matthew N. Idso,[†] Sunyia Hussain,[†] Matthias J. N. Junk,[†] Julia M. Fisher,[†] David D. Phan,[†] Songi Han,[†,‡] and Bradley F. Chmelka*[,†]

[†]Department of Chemical Engineering and [‡]Department of Chemistry and Biochemistry, University of California, Santa Barbara, California 93106, United States

Supporting Information

ABSTRACT: A versatile synthetic protocol is reported that allows high concentrations of functionally active membrane proteins to be incorporated in mesostructured silica materials. Judicious selections of solvent, surfactant, silica precursor species, and synthesis conditions enable membrane proteins to be stabilized in solution and during subsequent coassembly into silica−surfactant composites with nano- and mesoscale order. This was demonstrated by using a combination of nonionic (*n*-dodecyl-*β*-D-maltoside or Pluronic P123), lipid-like (1,2-diheptanoyl-*sn*-glycero-3-phosphocholine), and perfluoro-octanoate surfactants under mild acidic conditions to coassemble the light-responsive transmembrane protein proteorhodopsin at concentrations up to 15 wt % into the hydrophobic regions of worm-like mesostructured silica materials in films. Small-angle X-ray scattering, electron paramagnetic resonance spectroscopy, and transient UV−visible spectroscopy analyses established that proteorhodopsin molecules in mesostructured silica films exhibited native-like function, as well as enhanced thermal stability compared to surfactant or lipid environments. The light absorbance properties and light-activated conformational changes of proteorhodopsin guests in mesostructured silica films are consistent with those associated with the native H^+-pumping mechanism of these biomolecules. The synthetic protocol is expected to be general, as demonstrated also for the incorporation of functionally active cytochrome *c*, a peripheral membrane protein enzyme involved in electron transport, into mesostructured silica−cationic surfactant films.

INTRODUCTION

Proteins are versatile biomolecules that are tailored for particular functions in biological systems, many of which would be desirable to harness for technological applications. The compositions and structures of proteins within cellular environments have evolved under biological selection criteria for diverse functionalities, including highly selective reactions, molecular or ion transport, and signaling, which often occur at high rates and support the viabilities of biological organisms. Recently, there has been significant progress in the engineering of proteins to have functionalities that are different from those of wild-type analogues by judiciously adjusting protein compositions through biomolecular mutagenesis processes (e.g., directed evolution).[1,2] Many such functionalities could be attractive for technological uses, such as chemical or biological sensing,[3] catalysis,[4,5] separations,[6,7] bioanalytics,[8] or energy conversion,[9] though they are typically highly specific for certain substrates over a narrow range of conditions. The effective exploitation of proteins for nonbiological purposes often requires that proteins be extracted from native biological environments and stabilized in active forms within synthetic host materials. Such synthetic hosts should provide robust local environments for the protein molecules to function under abiotic conditions, over length scales larger than a single cell, and enable integration into technologically relevant processes or devices.

Membrane proteins in particular offer many technological opportunities based on their diverse functionalities, though incorporating them into synthetic host materials has been challenging due to their limited stabilities and high hydrophobicities that require robust amphiphilic host environments. Consequently, in contrast to water-soluble globular proteins, membrane proteins are generally located within or interact with the amphiphilic lipid bilayers that separate the interiors of cells from their surroundings. At these complicated interfaces, individual monomers or oligomeric assemblies[10−12] of membrane proteins regulate intracellular conditions in a variety of functional roles that include sensing, signal transduction, and the selective transport of ions or molecules,[13] many of which might be exploited for a variety of practical purposes. One interesting example is the membrane protein proteorhodopsin (PR), which is found ubiquitously in oceanic microorganisms[14−20] and which absorbs green light to actively transport H^+ ions (protons) across cell membranes as a part of cellular metabolic cycles.[19] On the basis of the photoresponsive transport activities of PR, synthetic materials that include PR

Received: July 2, 2017
Published: March 13, 2018

DOI: 10.1021/jacs.7b06863
J. Am. Chem. Soc. 2018, 140, 3892−3906

molecules have been proposed for a variety of energy conversion and optical applications, similar to those suggested for the homologous and well-characterized membrane protein bacteriorhodopsin of the archaea *Halobacterium salinarium*.[21−26] However, preparing synthetic hosts that contain membrane proteins with native or native-like activities is difficult, given the highly specific conditions required to support the generally complex protein structures[27,28] and dynamics[29,30] that are necessary for protein function. In most cases, membrane proteins can remain functional outside of the native lipid membranes only in the presence of membrane-mimetic surfactants or lipids[31−35] and over narrow ranges of solvent compositions and temperatures.[36] Such stability considerations have limited the incorporation of membrane proteins into only a few types of synthetic materials, including hydrogels,[37] block copolymers,[38−40] silica gels or glasses,[41,42] self-assembled lipid bilayer arrays,[43,44] and supported lipid bilayers.[45] These materials, however, exhibit poor processabilities and modest mechanical, thermal, and chemical stabilities that have limited their suitabilities for harnessing the functionalities of membrane proteins.[38,39,43−45]

The solution processabilities, amphiphilic properties, mechanical and thermal stabilities, and wide range of synthesis conditions of mesostructured silica make these materials advantageous to stabilize and exploit the functionalities of membrane proteins. Compared to lipid bilayers, mesostructured oxides are physically and chemically robust and can be synthesized with diverse mesoscopic (e.g., cubic, hexagonal, lamellar, or "worm-like") structures and macroscopic morphologies that include films, fibers, powders, and monoliths.[46] Furthermore, their mesoscale channel dimensions (3−12 nm) and specific volumes (1−2 cm^3/g) are suitable for macromolecular or colloidal guests, such as proteins,[5,8,47−51] conjugated polymers,[52,53] or nanoparticles.[54,55] For example, by adjusting the mesochannel diameters of mesoporous silica hosts to be within approximately 1 nm of the dimensions of a folded protein, such protein species could be stabilized within the host;[48,56] for the case of the water-soluble enzyme protein lipase, higher activities were observed for lipase molecules incorporated in mesoporous silica hosts with optimized mesochannel dimensions.[57] In addition, mesochannel surface compositions can be modified during syntheses or by postsynthetic treatments to facilitate the incorporation of such guests, e.g., by introducing protein binding sites[47] or by adjusting the hydrophobicity of the channel surfaces to promote interactions with proteins.[9,58] Despite such beneficial properties of mesostructured oxides, only a few types of membrane proteins, such as the light-harvesting photosynthetic complexes of the bacterium *Thermochratium tepidum*, have been incorporated in active forms into them, which has generally been achieved by the postsynthetic adsorption of proteins onto powders of these materials.[9,58,59] These approaches, however, lead to particles that often have composition gradients of proteins, small sizes (<10 μm diameters), and low interparticle connectivities, which limit the usefulness of powders in exploiting the molecular or ion transport properties of membrane proteins over macroscopic length scales.

Here, we present a general solution-based synthetic protocol for coassembling high concentrations of functional membrane proteins into surfactant-directed mesostructured silica materials as self-supporting films and monoliths. This is achieved by appropriate selection of solution compositions and conditions, including pH, solvent, and surfactant species that serve dual roles: to stabilize the large, highly hydrophobic, and relatively fragile membrane protein molecules and to direct their assembly with network-forming silica precursor species into a mesostructured silica composite. Proteorhodopsin was selected for incorporation, because its structure with seven α-helices represents a broad category of transmembrane proteins and because its light-activated functional properties are of potential technological interest. The structures, dynamics, stabilities, and distributions of PR guest molecules in synthetic mesostructured silica hosts are probed by a combination of complementary X-ray diffraction, electron paramagnetic resonance (EPR) spectroscopy, and optical absorbance analyses for comparison with those in native-like micellar solution (aq) and lipid environments. Insights into the light-responsive functionalities of PR species in mesostructured silica films are established from time-resolved EPR and visible absorbance analyses before and after pulsed illumination of the films with green light. Cationic surfactants were used to incorporate the peripheral membrane protein cytochrome *c* oxidase into mesostructured silica membranes to demonstrate the generality of the approach.

EXPERIMENTAL SECTION

Materials. Reagent grade tetraethoxysilane (TEOS, Aldrich Chemicals) was used as the silica precursor, and all acidic solutions were prepared by diluting concentrated hydrochloric acid (Fisher) with the appropriate amounts of deionized water. Amphiphilic surfactants were used to stabilize proteorhodopsin molecules in solution and to direct the formation of the PR-containing mesostructured silica composites. These included the nonionic surfactant *n*-dodecyl-β-D-maltoside (DDM, Anatrace), the triblock copolymer Pluronic P123 (poly(ethylene oxide)$_{20}$-*b*-poly(propylene oxide)$_{70}$-*b*-poly(ethylene oxide)$_{20}$), $(EO)_{20}(PO)_{70}(EO)_{20}$ (obtained as a gift from BASF, Mount Olive, New Jersey, USA), the zwitterionic lipid 1,2-diheptanoyl-*sn*-glycero-3-phosphocholine (diC_7PC, Avanti Polar Lipids), and the cationic surfactant tetradecyltrimethylammonium chloride (TTACl, TCI America, Portland, Oregon, USA). Ethanol (>99.5% purity, Gold Shield Distributors, Hayward, California, USA) was used as a cosolvent to incorporate PR into synthetic materials that used triblock copolymers as structure-directing species. Cytochrome *c* from equine heart was purchased from Sigma. The low-molecular-weight fluorinated surfactant, sodium perfluorooctanoate (PFO, Oakwood Products, Inc., West Columbia, South Carolina, USA) was used to promote macroscopically homogeneous distributions of PR in the films. The chemical formulas for these surfactants are shown in Figure 1A. All chemicals were used as-received.

Proteorhodopsin Preparation. The basic methodologies for expression, purification, and nitroxide spin-labeling of proteorhodopsin were implemented as described previously,[60,61] with further details given in the Supporting Information. The proteorhodopsin gene used here was the BAC31A8 sequence, modified such that the three natural cysteines were substituted with serine residues. The slowed-photocycle E108Q mutant was employed in light-triggered spectroscopic studies, and additional mutants with single cysteines were used for site-specific nitroxide-labeling and subsequent EPR characterization. Such cysteine residues, obtained by site-directed mutagenesis, were labeled with the commonly used methanethiosulfonate (MTSL) nitroxide moiety,[63,64] commonly termed R1, the structure of which is shown in Figure 1B. The two spin-labeled proteorhodopsin residues exploited in this study were located on the intracellular E−F loop of proteorhodopsin, as depicted schematically in Figure 1B, and characterized in detail elsewhere.[60] Proteorhodopsin species spin-labeled at either residue A174 or T177 were chosen, as they are associated with two modes of intraprotein contact (interfacial and exposed, respectively) and exhibit characteristic spectral signatures of light-driven conformational change, with those of A174R1 being larger in amplitude.[60]

DOI: 10.1021/jacs.7b06863
J. Am. Chem. Soc. 2018, 140, 3892−3906

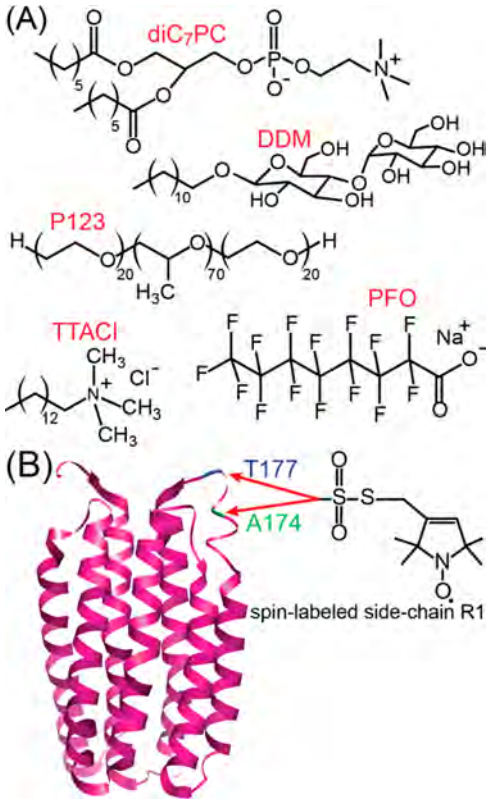

Figure 1. (A) Molecular structures of the structure-directing agents 1,2-diheptanoyl-3-glycero-*sn*-phosphocholine (diC$_7$PC), *n*-dodecyl-*β*-D-maltoside (DDM), Pluronic P123, and tetradecyltrimethylammonium chloride (TTACl) and the surfactant sodium perfluorooctanoate (PFO). (B) Schematic structure[62] of a proteorhodopsin monomer with the two specific residues A174 and T177 indicated to which nitroxide spin-labels (R1) were attached for EPR characterization.[60]

For this study, size-exclusion fast protein liquid chromatography (FPLC) was used to purify and isolate predominantly monomeric proteorhodopsin and to remove salt from the proteorhodopsin-containing solution to reduce the effects of excess ions on subsequent surfactant-directed coassembly of the mesostructured silica host. The separation of monomeric and oligomeric complexes of proteorhodopsin solubilized within DDM micelles has been previously demonstrated using a Superdex 200 FPLC column.[61] For the current investigations, before elution of the proteorhodopsin through the FPLC column, the proteorhodopsin was incubated overnight in buffer containing 2 wt % of the zwitterionic lipid-like diC$_7$PC, which was observed to enrich the monomeric fraction of PR when FPLC-purified with a 0.05 wt % DDM buffer.[10] After separation of the proteorhodopsin species by FPLC, the low-molecular-weight fractions corresponding to monomeric proteorhodopsin (with associated diC$_7$PC and DDM surfactants) were collected and concentrated by using 50,000 MWCO Amicon centrifugal filters (Millipore). All buffer compositions, up to and including the elution step of the purification, were 50 mM K_2HPO_4 and 150 mM KCl. To remove buffering salts, the monomeric PR solution was eluted through a Sephadex PD-10 buffer exchange column (GE Healthcare) equilibrated with Millipore water (18.2 MΩ·cm) containing 0.05 wt % DDM and adjusted to pH 4 using dilute HCl (aq). This was followed by centrifugation of the PR−surfactant solution using 50,000 MWCO Amicon centrifugal filters (Millipore) to obtain 60−1750 μM PR in solutions with volumes of 200−500 μL, as determined by optical absorbance.[32] Subsequent analyses of the resulting solutions by blue-native polyacrylamide gel electrophoresis revealed the presence of predominantly monomeric and dimeric proteorhodopsin species (63%, as estimated from the areas of the BN-PAGE signals, Supporting Information, Figure S1). Synthesis of materials with high (>10 wt %) protein loadings required the removal of excess DDM and diC$_7$PC surfactants from the monomeric PR FPLC fractions, which was achieved by binding the monomeric PR to Ni-NTA resin and subsequently washing the PR-bound resin with 200 mL of an aqueous buffer containing 0.05 wt % DDM buffer and 20 mM imidazole. After eluting PR from the Ni-NTA resin using 500 mM imidazole buffer, the K_2HPO_4, KCl, and imidazole salts were removed from the PR sample by eluting the PR through a Sephadex PD-10 buffer exchange column (GE Healthcare) equilibrated with Millipore water (18.2 MΩ·cm) containing 0.05 wt % DDM and adjusted to a pH of ∼4 using dilute aqueous HCl. The PR was then concentrated using 50,000 kDa MWCO Amicon centrifugal filters (Millipore) to the desired PR concentration.

Preparation of Protein-Containing Mesostructured Silica Films. DDM+diC$_7$PC-directed mesostructured silica materials without or with proteorhodopsin guests were typically synthesized by adding 0.05 g of tetraethoxysilane (TEOS) to 1 g of 4 mM HCl (aq) at room temperature. The mixture was stirred at room temperature for 2 h to allow the TEOS to hydrolyze, after which appropriate amounts of DDM, diC$_7$PC, and PFO were added, which direct the assembly of the mesostructured silica framework and stabilize monomeric proteorhodopsin species. After dissolution of these surfactants, the precursor solution was cast directly onto a suitable substrate (typically glass for optical characterization, a polymer, e.g., Kapton, for SAXS measurements, or PDMS to yield free-standing films) and allowed to dry under ambient temperature conditions in either ambient or relatively high controlled humidity for 2 days to generate the DDM+diC$_7$PC-directed mesostructured silica films before characterization. For materials that incorporate proteorhodopsin, the precursor solution was mixed in an approximately 1:1 ratio with an aqueous solution containing DDM +diC$_7$PC-solubilized proteorhodopsin monomers (60−1750 μM) prepared as described above, titrated to a desired pH between 3.5 and 5.2 using dilute HCl or NaOH, cast onto a desired substrate, and allowed to dry for 2 days under ambient conditions. The film thickness could be varied from a few microns (typically supported on a substrate) to that of a free-standing monolith with thicknesses ranging from approximately 50 μm to greater than 1 mm. The film area could also be controlled over arbitrary dimensions; films have been routinely prepared with areas of several square centimeters, with scaling to significantly larger film areas expected to be possible. High PR concentrations, relatively low (H_2O:TEOS mass ratio of <15:1) solvent quantities during synthesis, low (<25 wt %) silica content, and the presence of PFO promoted the assembly of mesostructured silica films with macroscopically uniform thicknesses and PR distributions (Supporting Information, Figure S2). DDM+diC$_7$PC-directed silica materials with 40 wt % DDM, 20 wt % diC$_7$PC, and 40 wt % SiO_2 were calcined by ramping the temperature at 0.5 °C/min to 550 °C, holding this temperature for 8 h, and subsequently decreasing the temperature to 25 °C at 4 °C/min.

Pluronic P123-directed mesostructured silica materials were similarly synthesized by first dissolving 0.7 g of P123 in 0.7 g of ethanol mixed with 0.6 g of 0.02 M HCl (aq). Following the dissolution of P123, 1.47 g of TEOS were added to this solution and allowed to hydrolyze for 2 h, after which 2.5 g of an aqueous solution containing the desired amount of proteorhodopsin (typically 80 μM) was added. This solution was then cast on a suitable substrate and allowed to dry at room temperature under a vacuum of 36 kPa to promote more rapid solvent evaporation.

To prepare mesostructured silica materials containing cytochrome *c*, 0.1 g of the structure-directing surfactant, TTACl, and 0.2 g of TEOS were mixed with 2 g of 5 mM HCl (aq), and the TEOS was allowed to hydrolyze for 2 h at ambient temperature. The pH of the resulting solution was approximately 4. After hydrolysis, 13.5 mg of cytochrome *c* was added. This mixed solution was then cast on a suitable substrate and allowed to dry under ambient temperature and humidity for 2 days.

Characterization. Small-angle X-ray scattering (SAXS) patterns were acquired from mesostructured silica−surfactant materials without or with proteorhodopsin to establish the degree of mesostructural

DOI: 10.1021/jacs.7b06863
J. Am. Chem. Soc. 2018, 140, 3892−3906

order in the films. Powders of DDM+diC$_7$PC-directed mesostructured films were characterized on a Rigaku Smartlab High-Resolution Diffractometer (λ = 1.542 Å, voltage 40 keV, current 44 mA). SAXS measurements of PR-containing P123-directed materials were conducted using a XENOCS Genix 50 W X-ray microsource with Cu Kα radiation (λ = 1.542 Å, voltage 50 keV, current 1 mA) and a MAR345 image plate area detector (located 1.4 m behind the sample) in a transmission geometry.

2D HYperfine Sublevel CORrelation (HYSCORE) pulsed EPR analyses were conducted to establish the proximities among the nitroxide spin-labels attached to E−F loop residue 174 of proteorhodopsin molecules and the ^{19}F moieties of sodium perfluoro-octanoate molecules in the mesostructured silica film. These pulsed-EPR experiments were performed at υ_L = 9.2492 GHz on an X-band Bruker Elexsys 580 spectrometer that was equipped with a Bruker Flexline split-ring resonator ER4118X-MS3. The temperature was set to 50 K by cooling with a closed-cycle cryostat (ARS AF204, customized for pulsed EPR, ARS, Macungie, Pennsylvania, USA). First, an electron spin−echo (ESE)-detected spectrum was recorded with the primary echo sequence $\pi/2-\tau-\pi-\tau-$echo. The lengths of the $\pi/2$ and π pulses were 16 and 32 ns, respectively, and τ was set to 200 ns. 2D HYSCORE spectra were recorded with the pulse sequence $\pi/2-\tau-\pi/2-t_1-\pi-t_2-\pi/2-\tau-$echo[65,66] at a magnetic field of 329.3 mT, corresponding to the maximum amplitude of the nitroxide EPR signal. The lengths of all pulses were set to 16 ns, and the time intervals t_1 and t_2 were varied from 300 to 4396 ns in increments of 16 ns. A standard eight-step phase cycle was used to eliminate unwanted echoes. To avoid substantial "blind spot" artifacts, two separate HYSCORE spectra were recorded with a τ value of either 148 or 180 ns. The time traces of each HYSCORE spectrum were baseline corrected with a third-order polynomial, apodized with a Gaussian window, and zero-filled with 1024 points along each dimension. After applying a two-dimensional (2D) Fourier transformation, the absolute-value spectra recorded for τ = 148 and 180 ns were then added to achieve an artifact-reduced spectrum.

Solution-state ^{1}H NMR measurements were conducted at 11.7 T on a Bruker AVANCE 500 MHz spectrometer operating at a ^{1}H frequency of 500.2 MHz. Single-pulse ^{1}H NMR spectra were acquired using a 90° pulse of 13.8 μs, an acquisition time of 6 s, and a recycle delay of 10 s for each of the 64 signal-averaged transients. The surfactant quantities in the desalted PR−surfactant solution were established by acquiring a solution-state single-pulse ^{1}H NMR spectrum on a solution containing 50 μL of the as-purified PR−surfactant sample and 950 μL of D_2O containing 0.1 wt % DDM, which corresponds to a 1-in-20 dilution of the PR−surfactant solution. The quantity of DDM in the diluted proteorhodopsin sample was obtained by comparing the integrated areas of the ^{1}H signals at 0.84, 3.5, and 5.4 ppm, assignable to the ^{1}H moieties of DDM,[67] to those from an external reference of 0.1 wt % DDM in D_2O.

Solid-state ^{19}F NMR spin−lattice T_1 relaxation time measurements were conducted at 11.7 T on a Bruker AVANCE II spectrometer and a 1.3 mm double-resonance Bruker magic-angle-spinning (MAS) probehead for fast sample rotation frequencies (54 kHz). To establish the interactions between the nitroxide spin-labels on proteorhodopsin and specific ^{19}F moieties of the PFO probe molecules, ^{19}F T_1 relaxation times were measured by a series of inversion−recovery experiments conducted at room temperature. Solid-state NMR ^{1}H{^{19}F} rotational-echo, double-resonance (REDOR) MAS NMR spectra were acquired at 9.4 T by using a variable-temperature 2.5 mm triple-resonance Bruker MAS probehead on a Bruker ASCEND-III NMR spectrometer operating at frequencies of 400.02 MHz for ^{1}H and 376.32 MHz for ^{19}F. Samples were packed into 2.5 mm zirconia rotors with Vespel caps. The ^{1}H{^{19}F} REDOR NMR spectra were acquired under MAS conditions of 15 kHz at approximately −20 °C, using a 6 s delay time, and 250 ms acquisition time for each of the 256 signal-averaged transients. A train of 15 rotor-synchronized π-pulses, corresponding to a 0.11 ms recoupling time, was applied to the ^{19}F channel to recouple the ^{19}F−^{1}H dipolar couplings during the ^{1}H evolution period. Differences among the signal intensities of spectra acquired without and with ^{19}F−^{1}H dipolar recoupling arise from the dipolar couplings among ^{1}H and ^{19}F moieties, providing insights about their proximities.

Continuous-wave (cw) EPR spectra were collected at room temperature with a 0.35 T Bruker EMXplus spectrometer equipped with a Bruker TE011 high-sensitivity cylindrical microwave cavity (ER 4119HS-LC High Sensitivity Probehead). The spectra were acquired using 20 mW incident microwave power, 1 G modulation amplitude, and 150 G sweep width on PR-containing mesostructured silica films or micellar solutions in 0.6 mm ID, 0.84 mm OD quartz capillaries (VitroCom) and placed into 4 mm diameter quartz EPR tubes (Wilmad). Multiple 40 s scans were averaged to enhance the signal-to-noise ratio of the EPR spectra.

Light activation of proteorhodopsin within the EPR microwave cavity was carried out by illumination through the cavity optical window using an ∼5 mW green (532 nm) diode laser (DPS20 Midwest Laser Products, LLC) that was mounted on an aluminum stage secured to the front of the electromagnet. Time-resolved laser-triggered cw EPR measurements were performed by synchronizing EPR data acquisition to a 500 ms laser flash from the green diode laser source, using a Hewlett-Packard 8116A pulse generator that provided TTL pulses to the external trigger port of the EMX-plus spectrometer and the diode laser with the desired timing. Transient changes of a specific cw EPR peak were tracked by fixing the magnetic field to resonate at the frequency of interest and observing the cw EPR spectral amplitude for 10−15 s during and after laser illumination by a 500 ms green laser pulse. Such measurements were repeated and averaged for 4 h or longer (1000 scans or more) to improve signal-to-noise.

Time-resolved optical absorbance measurements were conducted on a home-built apparatus previously described[60] and used to monitor the absorbance changes of proteorhodopsin guests induced by the green laser pulse. The same ∼5 mW green laser used for cw EPR experiments was used to illuminate the samples (silica films or solution), which were contained in a flat sample cell or a 1 mm square cuvette. A tungsten light source (Ocean Optics, LS-1) and a charge-coupled-device (CCD) camera (Andor Idus) were used to collect absorbance difference spectra every 80−100 ms after a 500 ms laser pulse. Buffers of identical compositions and monomeric proteorhodopsin were used to ensure that the photocycle kinetics measurements were comparable among all of the samples that were characterized.

Steady-state absorbance measurements were conducted on a Shimadzu UV3600 UV−vis-NIR spectrometer with an integrating-sphere detector to determine the thermal stability of proteorhodopsin molecules within the mesostructured silica films and in the lipid bilayer samples, as well as to examine the oxidation state of cytochrome *c*. The thermal stabilities of the various PR-containing samples were probed by heating samples for 24 h at the temperatures specified in the text (70−105 °C) in a Fisher Scientific IsoTemp oven. Ex situ absorbance measurements were performed following treatments at different temperatures and normalized to absorbance measurements on the same sample prior to heating; linear interpolation between the absorbances at 450 and 700 nm was used to estimate the baseline absorbance not attributable to the chromophore. Since negligible denaturation of PR was observed at 70 °C, these samples were also used to assess denaturation at 80 °C, but otherwise previously unheated samples were used in all tests. Samples of PR in lipid bilayers were prepared by the following procedure: overexpressing PR in *E. coli*, lysing these cells, using centrifugation to isolate the lipid membrane fragments, and then resuspending the lysed PR-containing membranes in a phosphate-buffered solution, as described in the Supporting Information.

UV−visible absorption analyses were also conducted to characterize the oxidation and reduction of cytochrome *c* guests in TTACl-directed mesostructured silica materials. For the UV−visible absorption measurements, the samples were prepared by placing a free-standing film of the material into a plastic cuvette and then incubating the film for 10 min in 2 mL of 0.1 M tris-acetate-buffered solution that was titrated to pH 7.0 by using 1 M HCl and without ethylenediaminetetraacetic acid. To reduce the cytochrome *c* guests in the mesostructured silica hosts, the tris-acetate-buffered solution in the

DOI: 10.1021/jacs.7b06863
J. Am. Chem. Soc. 2018, 140, 3892−3906

cuvette was removed and the film was subsequently incubated in 2 mL of a fresh tris-acetate-buffered solution with an otherwise identical composition, except with 30 mM ammonium iron(II) sulfate.

RESULTS AND DISCUSSION

Mesoscale Order in Proteorhodopsin-Containing Silica Films. The surfactants that stabilize proteorhodopsin molecules outside of the native lipid environments can also direct the assembly of mesostructured silica materials with or without proteorhodopsin. Surfactants such as the nonionic *n*-dodecyl-*β*-D-maltoside (DDM) and zwitterionic 1,2-diheptanoyl-*sn*-glycero-3-phosphocholine (diC$_7$PC) interact with PR species and enable the native structures, dynamics, and functionalities of these biomolecules to be preserved in non-native environments. We hypothesized that the PR-stabilizing surfactant species DDM and diC$_7$PC could direct the assembly of mesostructured silica materials, resulting in synthetic hosts into which functionally active PR guests could be incorporated. The structure-directing roles of DDM and diC$_7$PC surfactants, individually and in mixtures, were probed by small-angle X-ray scattering, which is sensitive to long-range order within the materials; for the X-ray wavelength used (1.54 Å), Bragg's law stipulates that small-angle (<5°) reflections correspond to periodicities larger than 1.5 nm, thereby providing information about mesoscale (2−50 nm, according to IUPAC convention) order within the surfactant-directed silica materials. For example, the SAXS pattern (Figure 2A) of a silica film synthesized with a mixture of DDM and diC$_7$PC surfactants in a 2:1 mass ratio shows a broad primary (*100*) reflection at 1.9° (full width at half-maximum, fwhm, 0.4°), corresponding to a *d*-spacing of 4.6 nm. The broadness of this reflection and the absence of higher-order Bragg reflections indicate the relatively modest long-range mesostructural organization of this DDM +diC$_7$PC-directed silica material. Similar films were also calcined and characterized by N_2 sorption and SEM analyses (Supporting Information, Figure S3), which establish a similar extent of mesostructural order and relatively uniform nanometer pore dimensions after calcination. These results are consistent with the proclivity of DDM surfactants to assemble into cylindrical aggregates[68] and suggest that DDM and diC$_7$PC form worm-like mesochannels within the mesostructured silica, as shown schematically in the inset of Figure 2A. The surfactant and silica compositions of DDM+diC$_7$PC-directed materials can be adjusted to produce materials with characteristic ordering length scales between 4 and 7 nm (Supporting Information, Figures S4−S7), with the smaller mesoscale dimensions observed for materials with higher diC$_7$PC contents, consistent with the shorter alkyl chains of the diC$_7$PC molecules compared to the DDM surfactant species. (The absence of DDM and diC$_7$PC from PR-containing solutions resulted in the precipitation of PR aggregates, which were unsuitable for forming transparent films containing high loadings of PR.) The worm-like mesostructural order represents a trade-off among the stabilizing effects of the relatively short-chain surfactants on proteorhodopsin guest molecules, the moderate hydrophilic−hydrophobic contrast of the short-chain surfactants, and the solution conditions (pH, solvent, temperature) required for coassembly of the surfactants with the network-forming silica and functionally active PR species.

Mesostructured silica synthesized with a 2:1 mass ratio of DDM to diC$_7$PC was selected to incorporate proteorhodopsin guest species, as these materials were expected to have

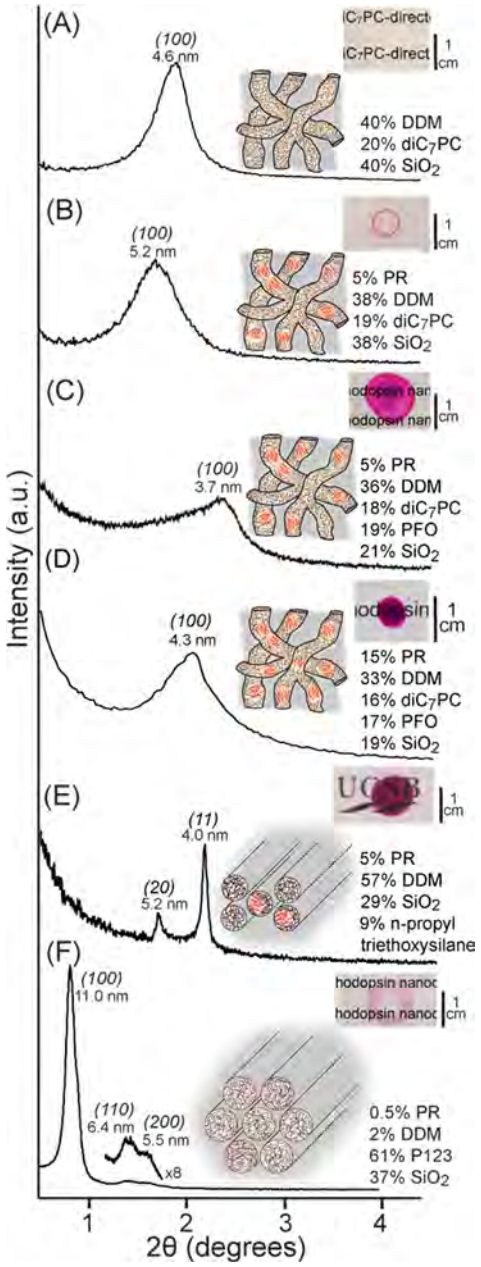

Figure 2. Powder small-angle X-ray scattering (SAXS) patterns and accompanying optical images of ca. 100 *μ*m thick DDM+diC$_7$PC-directed mesostructured silica films synthesized with different compositions on glass substrates: (A) without and (B) with 5 wt % proteorhodopsin (PR) incorporated; (C) with 5 wt % PR or (D) 15 wt % PR in DDM+diC$_7$PC+PFO-directed mesostructured silica films; and (E) with 15 wt % PR in a DDM-directed mesostructured silica film synthesized using a lower H_2O:TEOS ratio (3.5:15) and with 9 wt % of an organosilica precursor. (F) SAXS pattern of P123-directed mesostructured silica film containing 0.5 wt % PR. The schematic diagrams depict the relative dimensions of the silica mesochannels and proteorhodopsin in the different materials.

surfactant mesochannel dimensions (~4 nm) similar to those of proteorhodopsin monomers (~4 nm in length × ~3 nm in diameter, Figure 1B).[62] These DDM+diC$_7$PC-directed silica films synthesized with 5 wt % PR yielded a SAXS pattern with a single and somewhat broader primary (*100*) reflection at 1.7° (0.5° fwhm), corresponding to a *d*-spacing of 5.2 nm (Figure 2B) that is displaced to a smaller scattering angle compared to

DOI: 10.1021/jacs.7b06863
J. Am. Chem. Soc. 2018, 140, 3892−3906

otherwise identical silica films without PR guest species (Figure 2A). These observations are consistent with the incorporation of predominantly monomeric PR species in the DDM+diC_7PC-directed mesostructured silica host, which is expected to be associated principally with hydrophobic surfactant moieties in the silica mesochannels, owing to the high hydrophobicities of the membrane protein guests. However, these films often exhibited a coffee-ring-like gradient of PR loading, in which the periphery was transparent with an intense purple color (Figure 2B, inset), consistent with that of photoactive and functional PR under acidic conditions,[69] though with an inhomogeneous macroscopic distribution.

The homogeneities of the proteorhodopsin distributions and film thicknesses were significantly improved by synthesizing films with a third surfactant, perfluoro-octanoate (PFO, 19 wt %), with correspondingly less silica, and less acidic (pH 5) conditions (Supporting Information, Figure S8). This is thought to be due to more rapid condensation of silica at higher pH (compared to pH 4) and hydrophobic interactions between PFO and PR that inhibit the redistribution of PR molecules. Figure 2C shows a SAXS pattern for a mesostructured silica film containing 5 wt % PR synthesized with surfactant mass ratios of 2 DDM:1 diC_7PC:1 PFO, that exhibits a single SAXS reflection at 2.4° (0.3° fwhm), which corresponds to a *d*-spacing of 3.7 nm. The displacement of the reflection to a larger scattering angle, compared to the DDM +diC_7PC-directed materials without PFO, is consistent with the relatively high contents of diC_7PC and PFO, both of which have shorter alkyl chains than DDM and which are expected to lead to smaller mesochannel dimensions. Importantly, this film also manifests a uniform macroscopic distribution of PR, as shown in the optical image of the accompanying inset. In addition, nanoindentation analyses established that DDM +diC_7PC+PFO-directed mesostructured silica film with 5 wt % PR exhibited a mean hardness of 5.0 MPa and mean modulus of 260 MPa, both of which increase with silica content (Supporting Information, Table S1). These values are somewhat lower than reported for other mesostructured silica materials[70,71] though consistent with the lower silica content (21 wt %) of the DDM+diC_7PC+PFO-directed silica examined here. Higher loadings (15 wt %) of homogeneously distributed proteorhodopsin are notably achieved in mesostructured DDM +diC_7PC+PFO-directed silica films with the same surfactant mass ratios of 2 DDM:1 diC_7PC:1 PFO. As shown in Figure 2D, the resulting material yielded a SAXS pattern with a primary (*100*) reflection at 2.1° (0.5° fwhm) that corresponds to a *d*-spacing of 4.3 nm, consistent with expansion of the silica mesochannels to accommodate the PR guest species.

Synthesis compositions and conditions can be adapted to adjust the intermolecular interactions among the coassembling species and the resulting ordering, dimensions, and properties of proteorhodopsin-containing mesostructured silica hosts, although often with trade-offs. For example, DDM-directed silica synthesized with less water (mass ratio of 3.5 silica precursor:15 H_2O), with organosilica precursor species (e.g., *n*-propyltriethoxysilane), and with 5 wt % PR yielded narrow X-ray reflections at 1.7 and 2.0° (Figure 2E) that correspond to *d*-spacings of 5.2 and 4.0 nm, respectively. These are indexable to the (*20*) and (*11*) reflections of a rectangular phase, which has been reported for the binary DDM−water system,[72] though which would require additional higher order reflections to confirm. In addition, as shown in the accompanying inset, this high-silica film with 40 wt % SiO_2/*n*-propyl-$SiO_{1.5}$ showed no macroscopic cracks. By comparison, the use of conventional Pluronic P123, $(EO)_{20}(PO)_{70}(EO)_{20}$ triblock copolymer structure-directing surfactant species also yielded narrow reflections, though it was possible to incorporate only small quantities of PR (0.5 wt %) under the conditions used here. For example, the SAXS pattern in Figure 2F for P123-directed mesostructured silica containing 0.5 wt % PR shows three well-resolved reflections at 0.8° (0.1° fwhm), 1.3°, and 1.5° that are indexable to the (*100*), (*110*), and (*200*) reflections, respectively,[73] of a well-ordered hexagonal (*p6mm*) mesostructure with a unit cell parameter of 13.2 nm. Similar reflections are observed for otherwise identical P123-directed mesostructured silica film, except without PR (Supporting Information, Figure S7), consistent with the low PR content of the material and the relatively large mean mesochannel dimensions (ca. 8 nm diameter),[73] compared to the size of the PR monomers (Figure 2E). Higher concentrations (>0.5 wt %) of PR yielded pink powders that precipitated out of solution, exhibited no SAXS reflections (i.e., no mesostructural order was detectable), and from which macroscopic films could not be formed. These observations are likely due to the more hydrophilic characters of the ethylene oxide and propylene oxide blocks of the structure-directing P123 surfactant species compared to DDM or diC_7PC, the former of which are less compatible with and therefore less effective in incorporating the highly hydrophobic PR molecules under the synthesis conditions used.

Stability of Proteorhodopsin Molecules in Mesostructured Silica. The absorbance properties of proteorhodopsin guest species provide insight into their photoactivities and stabilities in synthetic mesostructured silica hosts. Under acidic conditions, the retinal chromophore within functional PR absorbs maximally at ∼546 nm,[69] which differs from the absorbance of free (non-PR-associated) retinal in aqueous solution at ∼380 nm.[74] This is a result of the different local environments of the retinal moieties within PR, including covalent and hydrogen bonding, as well as interactions with moieties in the H^+-ion channel of PR. The UV−visible absorbance spectrum in Figure 3A of a DDM+diC_7PC+PFO-directed silica film containing 5 wt % PR shows a broad (110 nm fwhm) absorption peak centered at 541 nm, which is characteristic of the retinal moieties in functionally active PR molecules under acidic conditions and accounts for the purple coloration of such films (Figure 2C, inset). This visible absorbance is absent in films without PR, prepared under otherwise identical compositions (Figure 3A, gray, see also the Supporting Information, Figure S9). Absorbance intensity is also observed in the range 350−450 nm, which likely originates from PFO molecules, scattered light from the mesostructured silica film, and/or the beta-band absorbance of the retinal chromophore in PR;[32,75] for bacteriorhodopsin, absorbance in this region is associated with high-energy transitions in the retinal that are separate from those associated with the chromophore absorbance above 500 nm.[76] Under ambient and dark storage conditions, the PR-containing mesostructured silica films retain purple colorations for at least several months, with no perceptible changes in absorbance detected by the human eye. Importantly, films with identical compositions, but prepared using synthesis conditions common for other mesostructured silicas (e.g., high acidity, high alkalinity, or with a cosolvent), appear yellow or transparent (Supporting Information, Figure S2), indicating that such conventional preparations have deleterious effects on the local structure and

DOI: 10.1021/jacs.7b06863
J. Am. Chem. Soc. 2018, 140, 3892−3906

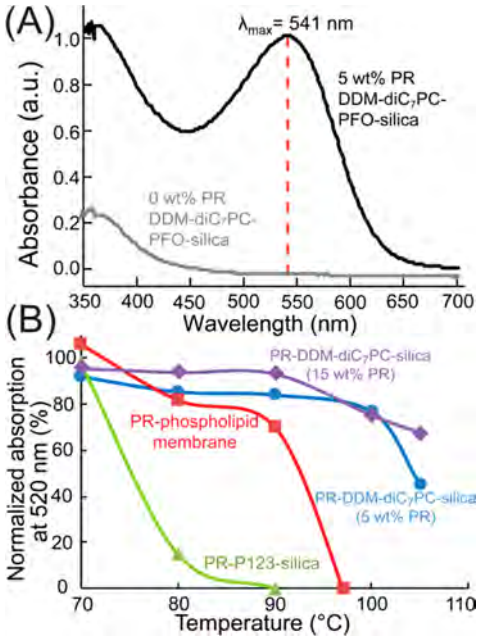

Figure 3. (A) UV−visible absorption spectrum of DDM+diC$_7$PC +PFO-directed mesostructured silica film without (gray) and with (black) 5 wt % of PR. Both spectra in part A were adjusted such that the absorbance at 900 nm was zero. (B) Normalized UV−visible absorbance intensities at 520 nm of proteorhodopsin in a mesostructured DDM+diC$_7$PC+PFO−silica film at 5 wt % (blue circles) and 15 wt % (purple diamonds), a mesostructured P123−silica film (green triangles), or in phospholipid membranes (red squares) after heating for 24 h at temperatures between 70 and 105 °C. For each heat-treated sample, the visible absorbance at 520 nm was measured and normalized to the absorbance intensity at 520 nm of the same sample measured before heating. The uncertainty in normalized absorption is expected to be 5−10% based on variations in film thicknesses and measurement limitations.

function of the PR chromophore. Collectively, these results demonstrate the stabilities of photoactive PR guests in DDM +diC$_7$PC+PFO-directed mesostructured silica host materials prepared under mildly acidic (pH 4−5) conditions and under ambient conditions.

In addition, proteorhodopsin guest molecules in DDM +diC$_7$PC+PFO-directed mesostructured silica films maintained high photoactivities after exposure to elevated temperatures (up to 105 °C). The thermal stabilities of photoactive PR guest species were assessed by measuring the absorbance intensities at 520 nm of PR-containing mesostructured DDM+diC$_7$PC +PFO-directed or P123-directed silica films after exposure to elevated temperatures up to 105 °C for 24 h. By Beer's law, these absorbance intensities are proportional to the concentration of photoactive PR guests; thus, their normalization to the 520 nm absorbance of each respective sample prior to thermal treatment yields an estimate for the percentage of PR guests that remain photoactive after each thermal treatment. For comparison, identical measurements and analyses were conducted on PR in native-like phospholipid membranes of *E. coli* cells. As shown in Figure 3, after thermal treatment at 70 °C, all four PR-containing materials retained at least 90% of the absorbance intensity at 520 nm, indicating a loss of <10% of photoactive PR species after heating to this moderately high temperature. After treatments at higher temperatures, however, significant differences were observed: there was no detectable absorbance at 520 nm from the PR-containing P123-directed silica film and *E. coli* membranes after heating to 90 and 97 °C, respectively, establishing that the PR guests in these materials were fully denatured within the sensitivity limits of the UV−visible absorbance analyses.

By comparison, after heating to an even higher temperature of 100 °C, the DDM+diC$_7$PC+PFO-directed silica films with 5 wt % PR retained 77% of the 520 nm absorbance observed in the film before thermal treatment, and 45% after heating at 105 °C for 24 h (Figure 3B, blue circles). Films with otherwise identical compositions but higher (15 wt %) PR loading showed similar 520 nm absorbance intensities (Figure 3B, purple diamonds) after thermal treatment, indicating a weak (if any) dependence of PR thermal stability on PR loading. The relatively high thermal stabilities of photoactive PR guests in the DDM+diC$_7$PC+PFO-directed silica, compared to the P123-directed films and phospholipid membranes, likely result from the combined benefits of the narrower DDM+diC$_7$PC+PFO-directed mesochannel dimensions (~3 nm) that physically constrain the PR species from unfolding and the favorable interactions between PR molecules and hydrophobic DDM, diC$_7$PC, and PFO surfactant moieties.

Local Proteorhodopsin Environments within Silica Mesochannels. Insight into the local distributions of proteorhodopsin guest molecules within the mesostructured silica hosts is provided by two-dimensional (2D) electron paramagnetic resonance (EPR) spectroscopy. EPR methods, such as hyperfine sublevel correlation (HYSCORE) experiments, are sensitive to hyperfine interactions between an electron spin and proximal (<1 nm) nuclear spins. Consequently, by exploiting a nitroxide spin-label ("R1") covalently attached to the exterior moieties of PR molecules (here, at the E−F loop site 174, "A174R1", Figure 1B), the local proximities of the spin-labels, and thus the attached PR molecules, to nearby nuclei can be probed. In the high-frequency (+, +) quadrant of a 2D HYSCORE spectrum, correlated intensities along the frequency diagonal arise from nuclear spins that are weakly coupled by hyperfine interactions to unpaired electrons, while the line shape of the correlated signal along the corresponding frequency *anti*-diagonal is related to the anisotropy associated with these interactions.

For example, the high-frequency quadrant of the 2D HYSCORE EPR spectrum (Figure 4) acquired on a DDM +diC$_7$PC+PFO-directed mesostructured silica film containing 5 wt % of spin-labeled PR-A174R1 shows correlated signal intensity along the diagonal at (14.0, 14.0) MHz. This corresponds to the ^{1}H nuclear Larmor frequency and establishes the close (<1 nm) proximities of ^{1}H moieties to the unpaired electrons of the nitroxide spin-labels attached to PR molecules. The antidiagonal line shape that intersects near (14.0, 14.0) MHz (labeled "^{1}H" in Figure 4) is similar to that of a characteristic powder pattern for an axially symmetric ^{1}H-electron hyperfine coupling tensor, the anisotropic parts of which result in the two less intense correlations separated evenly about the frequency diagonal at ca. (14.3, 14.3) MHz. The large ~1 MHz separation of these two signals about the frequency diagonal indicates that these signals arise from ^{1}H species that experience strong hyperfine couplings, allowing these signals to be confidently attributed to the strong *intramolecular* hyperfine interactions among the ^{1}H moieties and unpaired electron spin on each nitroxide spin-label. By comparison, the more intense and narrower frequency distribution near (14.0, 14.0) MHz likely originates from both intra- and intermolecular hyperfine interactions among a

DOI: 10.1021/jacs.7b06863
J. Am. Chem. Soc. 2018, 140, 3892−3906

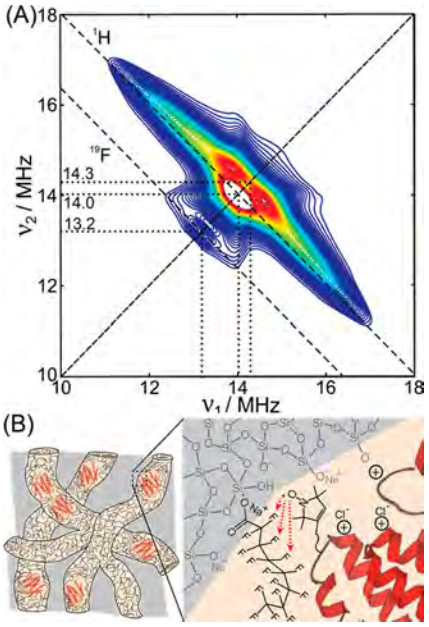

Figure 4. High-frequency region (A) of the 2D HYSCORE spectrum acquired from a DDM+diC$_7$PC+PFO-directed mesostructured silica film containing 5 wt % proteorhodopsin with a nitroxide spin-label at the E−F loop residue A174R1. The intensity at (13.2, 13.2) MHz is associated with the ^{19}F Larmor frequency at 0.3293 T and indicates the presence of ^{19}F spins, and thus PFO molecules, within 1 nm of the nitroxide spin-labels on the PR-A174 species, as shown in the schematic diagram in part B. This spectrum was acquired at a temperature of 50 K at a field strength of 0.3293 T and using a microwave frequency of υ_L = 9.2492 GHz.

large number of ^{1}H moieties of the protein and the surrounding environment that are more distant from the unpaired electrons. Signal intensity is also observed at (3.8, 3.8) MHz (Supporting Information, Figure S10), corresponding to the ^{13}C Larmor frequency, though it is very weak, due to the low (1.3%) natural abundance of ^{13}C nuclei in the protein and surfactant species in the mesostructured silica material.

The HYSCORE spectrum also provides detailed information about *intermolecular* interactions among the proteorhodopsin guest molecules with the surfactant and silica species of the mesostructured silica host material. In particular, the weaker correlated signal on the frequency diagonal at (13.2, 13.2) MHz, corresponding to the Larmor frequency of ^{19}F, unambiguously establishes the close proximities of the nitroxide spin-labels with ^{19}F nuclear spins of the PFO surfactant species, which are the only fluorinated molecules in this material. Separate solid-state ^{1}H{^{19}F} REDOR NMR experiments (Supporting Information, Figure S11) on mesostructured silica hosts without PR reveal the close (<1 nm) proximities of the hydrophobic perfluorinated chains of the PFO molecules and the alkyl chains of the stabilizing and structure-directing DDM and diC$_7$PC surfactant species. The HYSCORE and ^{1}H{^{19}F} REDOR analyses together indicate that spin-labeled PR species are close to and interact with the hydrophobic alkyl chains of the DDM and diC$_7$PC surfactant species that form the mesochannels of the mesostructured silica host. No correlated intensities are observed that suggest the close (<1 nm) proximities of the unpaired nitroxide electron spins and ^{29}Si nuclear spins of the silica framework, though the absence of signal could result from the low (4.7%) natural abundance of ^{29}Si nuclei and moderate silica content (20 wt %) in the material. In fact, under the relatively acidic (pH 3.5−5) synthesis conditions used for these materials, the intracellular side of PR would be positively charged[44] and thus be expected to interact with the negatively charged silica framework or extracellular regions of other PR guests. These analyses affirm that spin-labeled PR guest species are distributed within the DDM- and diC$_7$PC-rich surfactant channels of the mesostructured silica host, as depicted schematically in Figure 4B.

Dynamics of Proteorhodopsin within Mesostructured Silica. The light-activated H$^+$-transporting functionalities of proteorhodopsin molecules, whether within native lipid bilayers or within the mesostructured surfactant−silica host materials, rely on the dynamics of the PR molecules. Native cell membrane environments provide ample water, salts, and lipids to enable the conformational changes of PR molecules, specifically the pico- to nanosecond dynamics of protein structural elements that are thought to be generally necessary to support protein activities and biological functions.[77] Continuous-wave (cw) EPR is sensitive to such motions and therefore provides insight into the dynamics of PR within non-native host environments, which can have different length scales and compositions than in native lipids.

On the basis of the native-like optical absorption properties (Figure 3A) of proteorhodopsin molecules in synthetic mesostructured silica, we hypothesized that the surfactant-rich mesochannel environments would also support the native-like structural dynamics of proteorhodopsin guests. To test this hypothesis, cw EPR spectroscopy was used to examine the dynamics of nitroxide spin-labels attached to PR at residue A174 or T177 of the α-helical E−F loop (yielding PR-A174R1 or PR-T177R1, Figure 1B), the motions of which are highly correlated with the light-activated H$^+$-transport mechanism of PR.[60] The cw EPR spectra in Figure 5A of these spin-labeled PR species in powders of as-synthesized DDM+diC$_7$PC+PFO-directed mesostructured silica films exhibit line shapes that are characteristic of nitroxide radicals, with three distinct EPR peaks. Line shape analyses of the EPR spectra can provide site-specific information on the local dynamics of the spin-labeled moieties under different conditions.

Specifically, the line width of the central peak (characterized by H_0) is broader for less mobile species, while the intensities of the "*m*" and "*i*" components of the low-frequency peak (leftmost in Figure 5A) reflect the relative populations of nitroxide spin-labels that are relatively mobile and immobile, respectively, on the nanosecond time scale.[78,79] The "*m*" and "*i*" components may arise from spin-labels in two conformations that exchange slowly on the EPR time scale or not at all, due to differences in local PR structure or local molecular environments.

In particular, the dynamics of the E−F loop of proteorhodopsin in synthetic mesostructured silica hosts were evaluated by comparing the cw EPR line shapes of spin-labeled PR in DDM+diC$_7$PC+PFO-directed silica powders and in aqueous micellar solutions. The EPR spectra in Figure 5A acquired from PR-A174R1 or PR-T177R1 in as-synthesized DDM+diC$_7$PC+PFO-directed mesostructured silica both show center-peak line widths in the range 0.88−0.92 mT, which are broader than the 0.23−0.31 mT line widths (Figure 5B,C, insets) of identically spin-labeled PR in alkaline-buffered DDM +diC$_7$PC micellar solutions. These differences reflect the slower dynamics of the A174R1 and T177R1 side chains of PR guest molecules confined in mesostructured silica, compared to in DDM+diC$_7$PC micellar solutions. The slower side-chain

DOI: 10.1021/jacs.7b06863
J. Am. Chem. Soc. 2018, 140, 3892−3906

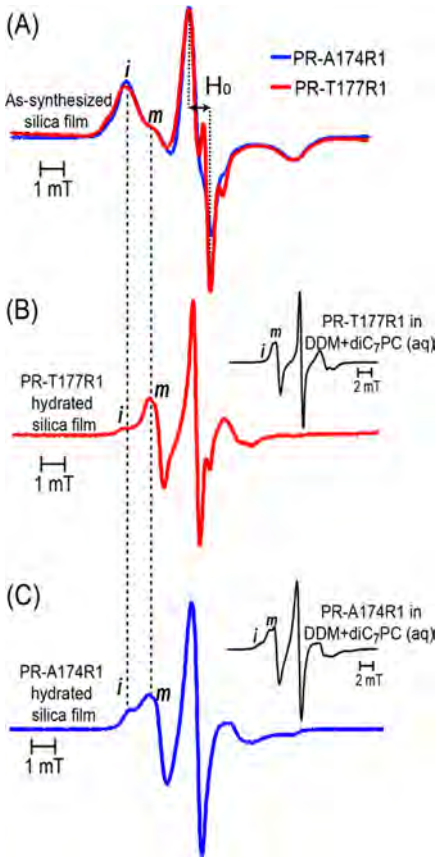

Figure 5. Continuous-wave EPR spectra of powders of DDM+diC$_7$PC +PFO-directed mesostructured silica films containing 5 wt % proteorhodopsin with nitroxide spin-labels at residues A174R1 or T177R1: (A) overlain spectra acquired from as-synthesized films, (B, C) spectra of the same mesostructured silica films containing either (B) PR-T177R1 or (C) PR-A174R1 hydrated in alkaline buffer (50 mM potassium phosphate, with 150 mM KCl, pH 9). The insets of parts B and C show the EPR spectra of the corresponding spin-labeled proteorhodopsin in alkaline-buffered DDM+diC$_7$PC micellar solutions under the same pH and buffer conditions.

dynamics for PR guest species in as-synthesized silica films are also qualitatively borne out in Figure 5A by the significantly greater EPR intensity of the low-frequency immobile "*i*" component over the mobile "*m*" component,[78,79] which is in contrast to the EPR spectra of otherwise identical PR in alkaline-buffered micellar solutions (Figure 5B,C insets) for which the reverse is observed. These results collectively indicate the slower dynamics of the E−F loop of proteorhodopsin molecules incorporated in as-synthesized DDM+diC$_7$PC+PFO-directed mesostructured surfactant−silica hosts, compared to native-like surfactant environments, consistent with physical confinement of the side chains of PR molecules within the ca. 5 nm silica mesochannels.

The side-chain dynamics of proteorhodopsin guest species in synthetic mesostructured silica depend strongly on the extent of hydration of the host material, as well. The EPR spectra (Figure 5B,C) of PR-containing mesostructured silica films hydrated by exposure to excess amounts of alkaline-buffered solutions (Figure 5B,C) show significantly higher relative signal intensities associated with the mobile "*m*" component (versus the immobile "*i*" component), compared to those of PR in as-synthesized films (Figure 5A). Nevertheless, the relative intensities of the mobile moieties in Figure 5B,C are still slightly less than those in spectra acquired from identically spin-labeled PR molecules in alkaline-buffered DDM+diC$_7$PC micellar solutions (Figure 5B,C insets). While these data reveal that the average side-chain dynamics of incorporated PR guests increase with hydration, native-like PR dynamics are not completely obtained even in fully hydrated films, likely due in part to the effects of confinement within the silica mesochannels. The mobile components in the EPR spectra of PR-A174R1 or PR-T177R1 guest species in P123-directed mesostructured silica films also increase with hydration (Supporting Information, Figure S12). Nevertheless, the EPR line shape analyses reveal that the side-chain mobilities of PR molecules in hydrated mesostructured silica host films are only slightly lower than PR in micellar solutions, suggesting that the proteorhodopsin guests maintain their predominant functional form. Despite the high mobilities of the PR species, the relatively high (30 wt %) silica contents of the host materials used for the EPR analysis appear to prevent the PR guests from leaching into buffered solutions, as established by UV−visible absorption spectroscopy (Supporting Information, Figure S13).

The different sensitivities of the spin-labeled A174R1 and T177R1 side-chain residues to hydration level yield structural information about the E−F loop of proteorhodopsin guests in the DDM+diC$_7$PC+PFO-directed mesostructured silica films. For PR with native folding, the amphiphilic E−F loop has an α-helical structure that is oriented along the cytoplasmic protein surface, with one side nearer to the protein bilayer and the other more exposed to solvent;[60,80] as a consequence, E−F loop residues closer to the bilayer, such as A174, show lower mobilities compared to residues farther from the bilayer, such as the solvent-exposed T177.[60] Upon hydrating as-synthesized PR-containing DDM+diC$_7$PC+PFO-directed mesostructured silica films, the spectral line widths (H_0, Figure 5B,C) decrease by factors of 2.1 and 3.4 for films containing PR-A174R1 and PR-T177R1, respectively, indicating that the T177R1 residue is more solvent-exposed than the A174R1 residue. This trend is consistent with the relatively greater solvent exposure for the T177R1 residue, versus the A174R1 residue, of PR molecules in native-like micellar solutions,[43] suggesting that the E−F loop of PR in hydrated mesostructured silica hosts retains its native-like fold.

Photoactivated Responses of Proteorhodopsin in Silica Mesochannels. The light-activated transient absorbance behaviors of proteorhodopsin species in mesostructured silica relate to and provide information about the H$^+$-pumping functionalities of these biomolecular guests. After excitation by green light, PR molecules in native environments undergo a photochemical reaction cycle that involves several changes in retinal isomerization, protein conformation, and the protonation states of various residues that result in the net transport of H$^+$ ions across the transmembrane region of PR.[81] As some of these changes yield different chemical and physical environments for the retinal chromophore, several intermediates in the reaction cycle have characteristic optical absorbance signatures.[32,82] For example, PR in the important "*M*" intermediate state, in which the Schiff base linkage of the retinal chromophore is deprotonated, absorbs maximally at 405 nm,[83] manifesting a significant blue-shift from the ~520 nm absorbance maximum of PR prior to light activation, referred to as the "*PR*" state. Additional photocycle intermediates include the "*K*" and "*N*" intermediates, which have characteristic absorbances that are red-shifted compared to the *PR* state.[69,83] As a result, after activation by green light, the transient

DOI: 10.1021/jacs.7b06863
J. Am. Chem. Soc. 2018, 140, 3892−3906

absorbance responses of PR-containing mesostructured silica can provide insights into the photochemical reaction cycle, and thus the H^+-ion pumping function, of PR guest species.

Light-triggered transient absorption analyses were conducted on PR-containing DDM+diC$_7$PC-directed mesostructured silica and compared with the light-activated absorbance responses of PR in DDM+diC$_7$PC micellar solutions, as well as in *E. coli* membranes. In this study, measurements were conducted using PR with the "proton donor" glutamate (E108) residue substituted to glutamine (Q), which prolongs the *M* photointermediate lifetime to seconds, compared to milliseconds in wild-type PR,[82] and enables the transient absorbance responses of PR to be observed by using conventional laser and optical spectroscopy analyses. In particular, key information about intermediates in the photochemical reaction cycle of proteorhodopsin species in the synthetic mesostructured silica films can be obtained from optical-absorbance difference spectra.[83] Such spectra are obtained by subtracting an absorbance spectrum collected for a sample 130 ms after activation by a 500 ms green laser pulse (~5 mW) from a spectrum acquired immediately prior to illumination; the intensities in such difference spectra manifest absorption changes that are associated with photoactivation. For example, the difference spectra in Figure 6A of 5 wt % PR-E108Q in both the mesostructured DDM+diC$_7$PC−silica films hydrated in alkaline buffers and alkaline-buffered DDM+diC$_7$PC micellar solutions show negative intensities at wavelengths near 520 nm, where the *PR* state absorbs, and positive intensities near wavelengths of 410 nm, where the *M* intermediate absorbs. These spectral features are consistent with a depleted population of PR species in the *PR* state, accompanied by an increased population of PR molecules in the *M* intermediate state at 130 ms after the green laser pulse. However, the spectrum (Figure 6A, red) of PR-E108Q in the hydrated mesostructured DDM+diC$_7$PC+PFO−silica film shows positive intensity at approximately 620 nm, where the red-shifted *K* or *N* intermediates absorb, while no such intensities are observed for PR-E108Q in alkaline-buffered DDM+diC$_7$PC micellar solutions (Figure 6A, black) in this wavelength region. These different transient absorbance behaviors reflect the different rates of accumulation and decay of the *K* and/or *N* intermediates[83] of PR in DDM+diC$_7$PC-mesostructured silica, compared to the micellar solution, possibly due to the somewhat lower extent of hydration and/or more acidic local environments of PR guests in the mesostructured silica. This is corroborated by a similar increase in intensity near 620 nm in the difference spectrum (Supporting Information, Figure S14) acquired from PR-E108Q in an otherwise identical as-synthesized mesostructured DDM+diC$_7$PC+PFO−silica film but prior to hydration and alkaline-buffering. Collectively, the transient optical absorbance analyses provide evidence, after illumination, of transient PR photointermediates in hydrated mesostructured silica hosts that are associated with light-activated H^+-pumping activity.

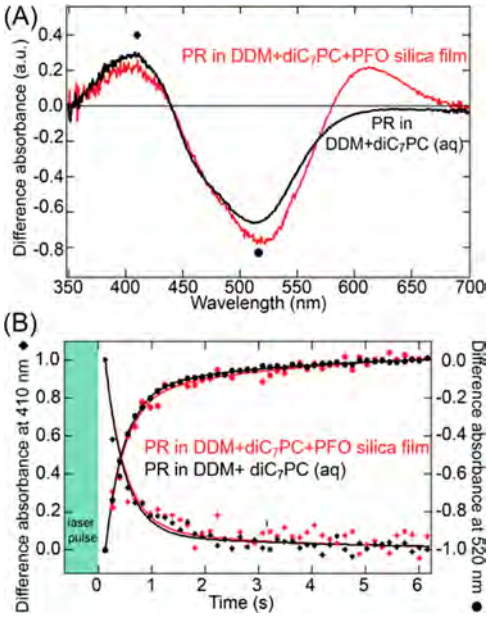

Figure 6. (A) Optical-absorbance difference spectra of the proteorhodopsin mutant PR-E108Q (also with the nitroxide R1 at residue A174C) in a DDM+diC$_7$PC+PFO-directed mesostructured silica film with 5 wt % PR hydrated in alkaline buffer (red) and in an alkaline-buffered DDM+diC$_7$PC micellar solution (black). Each spectrum was obtained from the difference of spectra acquired from the PR-E108Q sample before and 130 ms after illumination with a 500 ms green (532 nm) laser pulse at ~5 mW. (B) Transient absorbances at 410 nm (diamonds) and 520 nm (circles) from PR-E108Q in the hydrated DDM+diC$_7$PC+PFO-directed mesostructured silica film (red circles and diamonds) and in alkaline-buffered DDM+diC$_7$PC solution (black circles and diamonds), following a green laser pulse. The solid red and black lines in part B are biexponential fits of the transient absorption data. The alkaline buffer was composed of 50 mM potassium phosphate and 150 mM KCl at pH 9.

The photocycle kinetics of proteorhodopsin guests in synthetic mesostructured silica hosts also show similarities to monomeric proteorhodopsin in micellar solutions. Importantly, the time scales of the photointermediates determine the H^+-pumping rate of PR, with shorter time scales yielding higher proton-pumping rates that would be desirable for photoelectrochemical energy conversion applications. Here, the apparent interconversion kinetics of the *M* intermediate and *PR* states are estimated from the transient absorbances at wavelengths of 520 and 410 nm, respectively, at times 130 ms after green-laser excitation. As shown in Figure 6B, after illumination, the transient optical absorbance spectra of PR-E108Q in a DDM+diC$_7$PC+PFO-directed mesostructured silica film hydrated with alkaline buffer and monomeric PR-E108Q in an alkaline-buffered DDM+diC$_7$PC micellar solution both show transient decreases in intensities at 410 nm and concomitant increases in intensities at 520 nm. These results indicate a transient decrease in the population of PR in the *M* intermediate state and corresponding accumulation of the *PR* state, the interconversion time scales of which can be estimated by mathematical fitting of transient absorbance spectra. The *M* photointermediate states of PR and bacteriorhodopsin are commonly observed to decay biexponentially, with the two time scales arising from separate *M* intermediates, M_1 and M_2, that exhibit similar absorbances, but are thought to have distinct conformations with different proton accessibilities at the cytoplasmic interfaces of cell membranes.[83,84] Biexponential fits to the 410 nm absorbances shown in Figure 6B yield decay time scales for the respective M_1 and M_2 intermediates of 0.36 ± 0.01 and 3.2 ± 0.2 s for PR in the hydrated mesostructured DDM+diC$_7$PC+PFO surfactant−silica film and 0.36 ± 0.03 and 4.3 ± 0.7 s for PR in the alkaline-buffered DDM+diC$_7$PC micellar solution. The similar time scales of these transient absorbance behaviors imply similar H^+-ion transport rates for PR molecules in the mesostructured silica films and in native-

DOI: 10.1021/jacs.7b06863
J. Am. Chem. Soc. 2018, 140, 3892−3906

like micellar solutions (and also in extracted *E. coli* membranes, Supporting Information, Figure S15). Furthermore, as prior studies showed that the *M* intermediate decay rate is significantly different for monomeric and oligomeric PR species, with a 5× faster decay for PR monomers, the similar absorbance behaviors strongly suggest that predominantly monomeric PR species are incorporated in the mesostructured silica films.[10] The close correlation of the photocycle kinetics of PR in mesostructured silica films and in native-like micellar solutions thus indicates that PR guest molecules in mesostructured films are functionally active and perform comparably to PR in near-native environments.

EPR line shape analyses can provide additional and complementary information regarding the nature of the conformational changes far from the retinal chromophore that proteorhodopsin undergoes in mesostructured silica hosts upon light activation. To mediate the light-activated H^+-transport mechanism, PR molecules have been suggested to undergo a number of large-scale conformational changes that involve movements and torsions of secondary structural elements,[81] including the α-helical E−F loop that exhibits characteristic rigid-body movements associated with the *M* intermediate state decay.[60] Insights into these E−F loop motions can be obtained by monitoring the EPR line shapes of spin-labeled A174R1 residues of the E−F loop, which change significantly after photoactivation, due to the distinctively hindered dynamics of this residue caused by interactions with nearby residues at the cytoplasmic interface.[60] For example, the EPR spectrum of PR-A174R1 in a hydrated DDM+diC$_7$PC +PFO-directed mesostructured silica film under constant illumination by green light (Figure 7A, green traces) exhibits increased intensity associated with the relatively immobile "*i*" component and decreased intensity from the more mobile "*m*" component, compared to spectra acquired without light activation (Figure 7A, black traces, also shown in Figure 5C). Similar light-activated EPR signal responses are observed for PR-A174R1 in native-like DDM+diC$_7$PC micellar solutions and in P123-directed mesostructured silica films (Supporting Information, Figure S16). These results indicate that the A174R1 residues, as part of the E−F loop of PR guests in mesostructured silica, are on average more confined during light activation, consistent with the twisting and partial immobilization of the α-helical E−F loop of proteorhodopsin in response to light, as reported in previous studies of PR molecules incorporated in lipid bilayers.[60] Kinetic information about the E−F loop movements of proteorhodopsin can be obtained by transiently monitoring the EPR amplitudes of the relatively immobile "*i*" spectral component during and after light activation. As shown in Figure 7B (black trace), for PR-A174R1-E108Q in a DDM+diC$_7$PC-directed mesostructured silica film, the amplitude of the immobile EPR component increases during illumination by the green laser and subsequently decays after the laser is turned off. Similar transient EPR changes are observed for PR-A174R1-E108Q in an alkaline-buffered DDM+diC$_7$PC micellar solution (Figure 7B, gray trace). However, the decay of the immobile EPR component of PR-A174R1 after the laser pulse is faster for PR in the DDM+diC$_7$PC+PFO-directed mesostructured silica, reflecting faster E−F loop motions than in micellar solution. The faster E−F loop movements of PR molecules in the synthetic silica host may originate from confinement or interactions of PR molecules in the mesochannel environments that make the nonactivated PR state energetically more

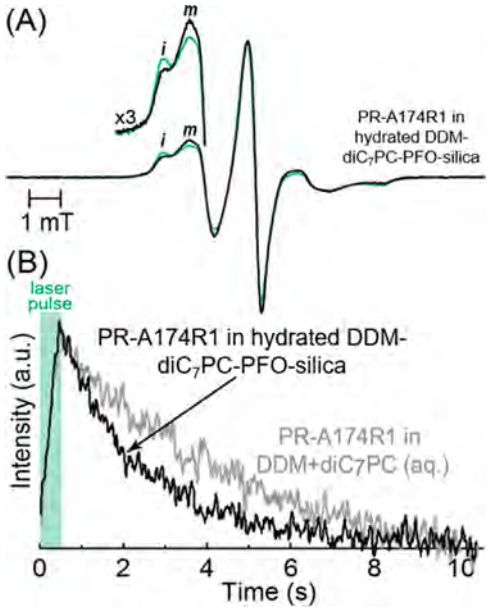

Figure 7. (A) Continuous-wave EPR spectrum acquired from powders of a DDM+diC$_7$PC+PFO-directed mesostructured silica film with 5 wt % PR-A174 hydrated with an alkaline (pH 9) buffered solution (50 mM potassium phosphate, 150 mM KCl) under continuous green laser illumination (green trace) and without illumination (black trace, also in Figure 5C). The inset in part A shows a zoomed in view of the spectral region with the immobile ("*i*") and mobile ("*m*") spectral components. (B) Transient EPR amplitudes at the frequency corresponding to the relatively immobile (*i*) component of the EPR spectra of PR-A174R1 in hydrated DDM+diC$_7$PC+PFO-directed mesostructured silica films (gray line) and in the alkaline-buffered (pH 9) DDM+diC$_7$PC micellar solution (black line), directly following illumination of these samples with a green laser (∼5 mW) pulse for 500 ms.

favorable than those of the photocycle intermediates. Such effects on the spin-labels of residue A174 of light-activated PR in the mesostructured silica hosts are consistent with those of nonilluminated PR guests discussed above (Figure 5). Given the native-like transient absorbances of PR in hydrated DDM +diC$_7$PC+PFO-directed mesostructured silica (Figure 6B), these data suggest that the large-scale E−F loop motions of light-activated PR guests are more sensitive to confinement in the mesochannel environment than changes that occur near the retinal chromophore. Interestingly, the transient changes in EPR spectra of PR-A174R1 in P123-directed mesostructured silica are nearly identical to those in DDM+diC$_7$PC micellar solution (Supporting Information, Figure S16), demonstrating that the kinetics of the light-activated E−F loop conformational transformation are not faster for PR incorporated into the larger P123-directed silica mesochannel environments. The detailed time-resolved EPR spectroscopy results show that site-specifically labeled PR molecules in synthetic mesostructured silica host materials undergo large-scale native-like conformational changes associated with the light-induced H^+-transport properties of PR, the kinetics of which may be enhanced by confinement.

Incorporation of Cytochrome *c* in Mesostructured Silica Hosts. The synthetic protocol presented here can be adapted to incorporate other functionally active membrane proteins within synthetic mesostructured silica hosts. To demonstrate this, we adjusted the synthesis protocol to incorporate the more hydrophilic protein cytochrome *c*, an

DOI: 10.1021/jacs.7b06863
J. Am. Chem. Soc. 2018, 140, 3892−3906

iron-containing biomacromolecule (~12 kDa) associated with the mitochondria in cells. In contrast to proteorhodopsin, which is a transmembrane protein that spans the lipid bilayer, cytochrome *c* is a peripheral membrane protein that is water-soluble and, thus, is not found within lipid bilayers but rather associates with integral membrane proteins at lipid bilayer surfaces.[85] Cytochrome *c* molecules were incorporated into surfactant-directed mesostructured silica host materials by using the cationic surfactant tetradecyltrimethylammonium chloride (TTACl). The SAXS pattern in Figure 8A of a TTACl-directed mesostructured silica film without cytochrome *c* shows two reflections at 2.3° (0.15° fwhm) and 3.9° that are indexable to the (*100*) and (*110*) reflections, respectively, of a well-ordered hexagonal mesostructured material with a lattice parameter of 4.6 nm. By comparison, the SAXS pattern for an otherwise identical TTACl-directed silica film containing 8 wt % cytochrome *c* exhibits a single broad reflection at 2.1° (0.5° fwhm) that corresponds to a *d*-spacing of 4.2 nm, a 0.3 nm increase with respect to the (*100*) *d*-spacing (3.9 nm) of materials without cytochrome *c*. As cytochrome *c* molecules are approximately spherical in shape with a diameter of 3 nm, the observed 0.3 nm increase in the characteristic ordering length scale is consistent with the expansion of the mesostructured silica framework upon incorporation of cytochrome *c* guests. In addition, the (*100*) reflection is substantially broader for the mesostructured silica containing 8 wt % cytochrome *c*, reflecting less mesostructural order, compared to the material without protein. The amphiphilic globular cytochrome *c* molecules likely reside near the mesochannel surfaces of the relatively hydrophilic silica framework and trimethylammonium moieties of the TTACl-directed mesostructured host, as depicted schematically in the inset of Figure 8A. These results are similar to those for proteorhodopsin guest species in DDM +diC$_7$PC-directed mesostructured silica, in which increased extents of membrane protein incorporation are associated with larger *d*-spacings and reduced mesostructural order. Interestingly, the TTACl-directed mesostructured silica with 8 wt % cytochrome *c* shows an additional broad reflection at 0.85°, which corresponds to a *d*-spacing of 10.3 nm that is significantly larger than the 4.2 nm *d*-spacing of the assigned (*100*) reflection. This low-angle reflection may originate from the incorporation of cytochrome *c* oligomers, which have been reported to readily form in the presence of ethanol,[86] which is produced by hydrolysis of TEOS precursor species during coassembly of TTACl-directed mesostructured silica.

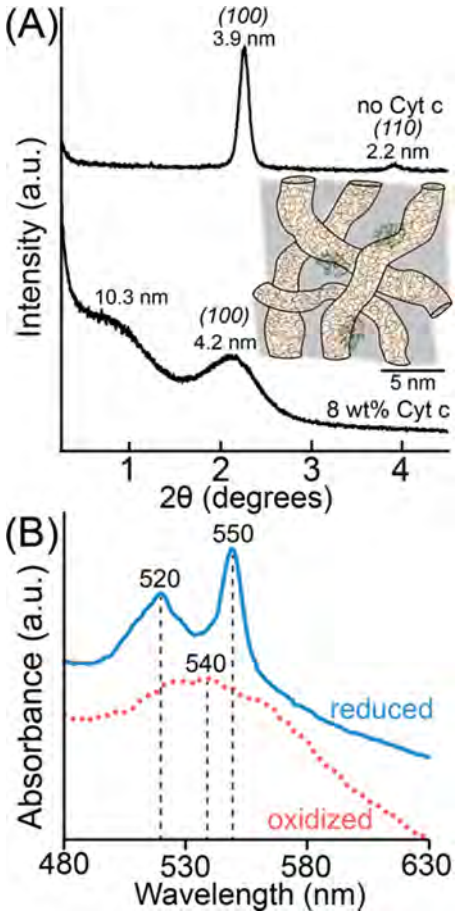

Figure 8. (A) Small-angle X-ray scattering patterns for a TTACl-directed silica film without (top) and with (bottom) 8 wt % cytochrome *c* that shows one reflection assigned to the (*100*) reflection of a worm-like mesostructure with a *d*-spacing of 4.2 nm. (B) Visible absorbance spectra collected from the same cytochrome-*c*-containing mesostructured silica film soaked in a tris-acetate buffer solution at neutral pH before (dotted red) and 10 min after (solid blue) the addition of 30 mM ammonium iron(II) sulfate.

The activities of cytochrome *c* guests in the mesostructured silica hosts were assessed by using optical absorbance spectroscopy, which is sensitive to the oxidation states of the iron centers of cytochrome *c* molecules. Cytochrome *c* oxidase species are capable of undergoing oxidation or reduction as part of the electron transport processes in mitochondria.[87] The oxidized and reduced states of cytochrome *c* in aqueous solutions notably manifest distinct optical absorbance signatures, with the reduced state exhibiting absorption maxima at ca. 520 and 550 nm and the oxidized state at ca. 532 nm.[88,89] Accordingly, the optical absorbance spectrum in Figure 8B of a TTACl-directed silica film exposed to a buffered solution at neutral pH (Figure 8B, dotted red) shows a broad absorbance maximum at ca. 540 nm, characteristic of the oxidized state of cytochrome *c*. By comparison, after soaking the film in the same buffer but containing 30 mM ammonium iron(II) sulfate (aq), the broad absorbance near 540 nm disappears and new narrower absorbances are observed at ca. 520 and 550 nm (Figure 8B, blue), characteristic of the reduced state of cytochrome *c*. These results demonstrate that cytochrome *c* molecules in TTACl-directed mesostructured silica films are accessible to diffusing species within the host channels, adopt native-like oxidation and reduction states, and retain their functional activities.

■ CONCLUSIONS

The judicious selection of material compositions and processing conditions enabled high concentrations (15 wt %) of the light-activated membrane protein proteorhodopsin (PR) to be incorporated in functionally active forms in mesostructured surfactant−silica host materials. Mixtures of DDM surfactants with either diC$_7$PC zwitterionic lipids, P123 triblock copolymers, or PFO were shown to serve jointly to both stabilize the hydrophobic PR molecules in aqueous solutions and direct their assembly and that of network-forming silica species into mesostructured silica composites. The solution processing conditions enabled PR-containing mesostructured silica materials to be prepared as transparent, colored, mechanically stable films or monoliths of up to 1 mm thickness and arbitrary lateral macroscopic dimensions. Proteorhodopsin

DOI: 10.1021/jacs.7b06863
J. Am. Chem. Soc. 2018, 140, 3892−3906

in DDM+diC$_7$PC+PFO−silica mesostructured materials were shown to exhibit comparable optical absorbance properties as native-like PR but with significantly enhanced thermal stabilities compared to photoactive PR in native-like phospholipid bilayers of *E. coli* or P123-directed silica hosts. Small-angle X-ray scattering and 2D HYSCORE EPR spectroscopy results showed that hydrophobic PR guest molecules were distributed within the hydrophobic surfactant mesochannels, as opposed to the hydrophilic silica framework. The dynamics of the functionally important E−F loop of the PR guests in DDM +diC$_7$PC+PFO-directed silica materials depended on the extent of hydration and confinement within the mesochannel environments, with fully hydrated materials supporting E−F loop dynamics similar to those in native-like DDM+diC$_7$PC micellar solutions. The transient photoresponses of PR guest molecules in the hydrated mesostructured silica host materials were demonstrated to be similar to those associated with light-activated H^+-ion transport by PR in near-native environments under alkaline conditions. These results thus establish that the PR guest molecules retain their native-like structures and light-activated dynamics, which indicate that they retain their functional properties. This opens the intriguing possibility to generate macroscopic H^+ gradients, provided that macroscopic orientational order can be imposed on an ensemble of PR guest molecules in the films, which we are currently pursuing in our laboratory. Adaptation of synthesis compositions and conditions (e.g., structure-directing surfactant type) enabled high (8 wt %) concentrations of the relatively hydrophilic membrane protein cytochrome *c* oxidase to be incorporated into hexagonally ordered mesostructured silica materials, while maintaining native-like oxidation and reduction activities (for which macroscopic orientational ordering of the membrane protein guests is not essential). The generality of this synthetic approach is expected to open new opportunities for developing materials that exploit the high selectivities and diverse functions of membrane proteins for applications in separations, sensors, catalysis, regulated delivery, and ion transport, including by photoactivation.

■ ASSOCIATED CONTENT

Supporting Information

The Supporting Information is available free of charge on the ACS Publications website at DOI: 10.1021/jacs.7b06863.

Protocols for expression, purification, and spin-labeling of proteorhodopsin, additional SAXS patterns, N_2 sorption data, SEM images, UV−visible spectra, EPR spectra, and a $^1H\{^{19}F\}$ REDOR spectrum for mesostructured silica−surfactant materials with diverse compositions (PDF)

■ AUTHOR INFORMATION

Corresponding Author

*bradc@engineering.ucsb.edu

ORCID

Songi Han: 0000-0001-6489-6246

Bradley F. Chmelka: 0000-0002-4450-6949

Notes

The authors declare no competing financial interest.

■ ACKNOWLEDGMENTS

This work was supported by the Institute for Collaborative Biotechnologies through grant W911NF-09-0001 from the U.S. Army Research Office and also partially by the National Institutes of Health under Grant No. R01GM116128. Characterization measurements were conducted using the Central Facilities of the UCSB Materials Research Laboratory supported by the MRSEC program of the US NSF under Award No. DMR-1720256. The pulsed EPR HYSCORE measurements were carried out at the Max Planck Institute for Polymer Research in Mainz, Germany. We thank A. Aye, N. Baxter, E. Chang, M. Kinnebrew, S. Narayanan, and N. Schonenbach for assistance with development of molecular biology and PR purification and expression protocols, B. Calloway for assistance with nanoindentation analyses, and Dr. A. Mikhailovsky for assistance with the time-resolved optical absorbance spectroscopy measurements in the shared user facilities of the UCSB Dept. of Chemistry and Biochemistry. J.P.J. thanks the CONVENE-IGERT program of the U.S. National Science Foundation for a doctoral fellowship under grant NSF-DGE 0801627. M.J.N.J. acknowledges financial support from the Alexander von Humboldt-Foundation through a Feodor Lynen Research Fellowship.

■ REFERENCES

(1) Engqvist, M. K. M.; McIsaac, R. S.; Dollinger, P.; Flytzanis, N. C.; Abrams, M.; Schor, S.; Arnold, F. H. *J. Mol. Biol.* **2015**, *427*, 205.

(2) Kan, S. B. J.; Lewis, R. D.; Chen, K.; Arnold, F. H. *Science* **2016**, *354*, 1048.

(3) Swift, B. J.; Shadish, J. A.; DeForest, C. A.; Baneyx, F. *J. Am. Chem. Soc.* **2017**, *139*, 3958.

(4) Shieh, F.-K.; Wang, S.-C.; Yen, C.-I.; Wu, C.-C.; Dutta, S.; Chou, L.-Y.; Morabito, J. V.; Hu, P.; Hsu, M.-H.; Wu, K. C.-W.; Tsung, C.-K. *J. Am. Chem. Soc.* **2015**, *137*, 4276.

(5) Hudson, S.; Cooney, J.; Magner, E. *Angew. Chem., Int. Ed.* **2008**, *47*, 8582.

(6) Wang, M.; Wang, Z.; Wang, X.; Wang, S.; Ding, W.; Gao, C. *Environ. Sci. Technol.* **2015**, *49*, 3761.

(7) Fane, A. G.; Wang, R.; Hu, M. X. *Angew. Chem., Int. Ed.* **2015**, *54*, 3368.

(8) Ispas, C.; Sokolov, I.; Andreescu, S. *Anal. Bioanal. Chem.* **2009**, *393*, 543.

(9) Oda, I.; Hirata, K.; Watanabe, S.; Shibata, Y.; Kajino, T.; Fukushima, Y.; Iwai, S.; Itoh, S. *J. Phys. Chem. B* **2006**, *110*, 1114.

(10) Hussain, S.; Kinnebrew, M.; Schonenbach, N. S.; Aye, E.; Han, S. *J. Mol. Biol.* **2015**, *427*, 1278.

(11) Maciejko, J.; Mehler, M.; Kaur, J.; Lieblein, T.; Morgner, N.; Ouari, O.; Tordo, P.; Becker-Baldus, J.; Glaubitz, C. *J. Am. Chem. Soc.* **2015**, *137*, 9032.

(12) Edwards, D. T.; Huber, T.; Hussain, S.; Stone, K. M.; Kinnebrew, M.; Kaminker, I.; Matalon, E.; Sherwin, M. S.; Goldfarb, D.; Han, S. *Structure* **2014**, *22*, 1677.

(13) Yoshizawa, S.; Kumagai, Y.; Kim, H.; Ogura, Y.; Hayashi, T.; Iwasaki, W.; Delong, E. F.; Kogure, K. *Proc. Natl. Acad. Sci. U. S. A.* **2014**, *111*, 6732.

(14) Béjà, O.; Aravind, L.; Koonin, E. V.; Suzuki, M. T.; Hadd, A.; Nguyen, L. P.; Jovanovich, S. B.; Gates, C. M.; Feldman, R. A.; Spudich, J. L.; Spudich, E. N.; DeLong, E. F. *Science* **2000**, *289*, 1902.

(15) DeLong, E. F.; Béjà, O. *PLoS Biol.* **2010**, *8*, e1000359.

(16) DeLong, E. F. *Nat. Rev. Microbiol.* **2005**, *3*, 459.

(17) de la Torre, J. R.; Christianson, L. M.; Béjà, O.; Suzuki, M. T.; Karl, D. M.; Heidelberg, J.; DeLong, E. F. *Proc. Natl. Acad. Sci. U. S. A.* **2003**, *100*, 12830.

(18) Sabehi, G.; Massana, R.; Bielawski, J. P.; Rosenberg, M.; DeLong, E. F.; Beja, O. *Environ. Microbiol.* **2003**, *5*, 842.

DOI: 10.1021/jacs.7b06863
J. Am. Chem. Soc. 2018, 140, 3892−3906

(19) Béjà, O.; Spudich, E. N.; Spudich, J. L.; Leclerc, M.; DeLong, E. F. *Nature* **2001**, *411*, 786.
(20) Moran, M. A.; Miller, W. L. *Nat. Rev. Microbiol.* **2007**, *5*, 792.
(21) Jensen, R. B.; Kelemen, B. R.; McAuliffe, J. C.; Smith, W. C. U.S. Patent 7,745,066, 2010.
(22) Luo, T.-J. M.; Soong, R.; Lan, E.; Dunn, B.; Montemagno, C. *Nat. Mater.* **2005**, *4*, 220.
(23) Bräuchle, C.; Hampp, N.; Oesterhelt, D. *Adv. Mater.* **1991**, *3*, 420.
(24) Chen, Z.; Birge, R. R. *Trends Biotechnol.* **1993**, *11*, 292.
(25) Bertoncello, P.; Nicolini, D.; Paternolli, C.; Bavastrello, V.; Nicolini, C. *IEEE Trans. Nanobioscience* **2003**, *2*, 124.
(26) Hampp, N. *Chem. Rev.* **2000**, *100*, 1755.
(27) Andreas, L. B.; Le Marchand, T.; Jaudzems, K.; Pintacuda, G. *J. Magn. Reson.* **2015**, *253*, 36.
(28) Andreas, L. B.; Jaudzems, K.; Stanek, J.; Lalli, D.; Bertarello, A.; Le Marchand, T.; Cala-De Paepe, D.; Kotelovica, S.; Akopjana, I.; Knott, B.; Wegner, S.; Engelke, F.; Lesage, A.; Emsley, L.; Tars, K.; Herrmann, T.; Pintacuda, G. *Proc. Natl. Acad. Sci. U. S. A.* **2016**, *113*, 9187.
(29) Becker-Baldus, J.; Bamann, C.; Saxena, K.; Gustmann, H.; Brown, L. J.; Brown, R. C. D.; Reiter, C.; Bamberg, E.; Wachtveitl, J.; Schwalbe, H.; Glaubitz, C. *Proc. Natl. Acad. Sci. U. S. A.* **2015**, *112*, 9896.
(30) Good, D. B.; Wang, S.; Ward, M. E.; Struppe, J.; Brown, L. S.; Lewandowski, J. R.; Ladizhansky, V. *J. Am. Chem. Soc.* **2014**, *136*, 2833.
(31) Lenz, M. O.; Huber, R.; Schmidt, B.; Gilch, P.; Kalmbach, R.; Engelhard, M.; Wachtveitl, J. *Biophys. J.* **2006**, *91*, 255.
(32) Friedrich, T.; Geibel, S.; Kalmbach, R.; Chizhov, I.; Ataka, K.; Heberle, J.; Engelhard, M.; Bamberg, E. *J. Mol. Biol.* **2002**, *321*, 821.
(33) Shi, L.; Lake, E. M. R.; Ahmed, M. A. M.; Brown, L. S.; Ladizhansky, V. *Biochim. Biophys. Acta, Biomembr.* **2009**, *1788*, 2563.
(34) Yang, J.; Aslimovska, L.; Glaubitz, C. *J. Am. Chem. Soc.* **2011**, *133*, 4874.
(35) Ranaghan, M. J.; Schwall, C. T.; Alder, N. N.; Birge, R. R. *J. Am. Chem. Soc.* **2011**, *133*, 18318.
(36) Scharnagl, C.; Reif, M.; Friedrich, J. *Biochim. Biophys. Acta, Proteins Proteomics* **2005**, *1749*, 187.
(37) Jeon, T.-J.; Malmstadt, N.; Schmidt, J. J. *J. Am. Chem. Soc.* **2006**, *128*, 42.
(38) Hua, D.; Kuang, L.; Liang, H. *J. Am. Chem. Soc.* **2011**, *133*, 2354.
(39) Ma, D.; Zhao, Y.; Wu, J.; Cui, T.; Ding, J. *Soft Matter* **2009**, *5*, 4635.
(40) Yang, Y. J.; Holmberg, A. L.; Olsen, B. D. *Annu. Rev. Chem. Biomol. Eng.* **2017**, *8*, 549.
(41) Ellerby, L. M.; Nishida, C. R.; Nishida, F.; Yamanaka, S. A.; Dunn, B.; Valentine, J. S.; Zink, J. I. *Science* **1992**, *255*, 1113.
(42) Wu, S.; Ellerby, L. M.; Cohan, J. S.; Dunn, B.; El-Sayed, M. A.; Valentine, J. S.; Zink, J. I. *Chem. Mater.* **1993**, *5*, 115.
(43) Liang, H.; Whited, G.; Nguyen, C.; Stucky, G. D. *Proc. Natl. Acad. Sci. U. S. A.* **2007**, *104*, 8212.
(44) Liang, H.; Whited, G.; Nguyen, C.; Okerlund, A.; Stucky, G. D. *Nano Lett.* **2008**, *8*, 333.
(45) Janshoff, A.; Steinem, C. *Anal. Bioanal. Chem.* **2006**, *385*, 433.
(46) Athens, G. L.; Shayib, R. M.; Chmelka, B. F. *Curr. Opin. Colloid Interface Sci.* **2009**, *14*, 281.
(47) Yiu, H. H. P.; Wright, P. A. *J. Mater. Chem.* **2005**, *15*, 3690.
(48) Washmon-Kriel, L.; Jimenez, V. L.; Balkus, K. J., Jr. *J. Mol. Catal. B: Enzym.* **2000**, *10*, 453.
(49) Lei, J.; Fan, J.; Yu, C.; Zhang, L.; Jiang, S.; Tu, B.; Zhao, D. *Microporous Mesoporous Mater.* **2004**, *73*, 121.
(50) Renault, C.; Balland, V.; Martinez-Ferrero, E.; Nicole, L.; Sanchez, C.; Limoges, B. *Chem. Commun.* **2009**, 7494.
(51) Wei, J.; Ren, Y.; Luo, W.; Sun, Z.; Cheng, X.; Li, Y.; Deng, Y.; Elzatahry, A. A.; Al-Dahyan, D.; Zhao, D. *Chem. Mater.* **2017**, *29*, 2211.
(52) Kirmayer, S.; Dovgolevsky, E.; Kalina, M.; Lakin, E.; Cadars, S.; Epping, J. D.; Fernández-Arteaga, A.; Rodríguez-Abreu, C.; Chmelka, B. F.; Frey, G. L. *Chem. Mater.* **2008**, *20*, 3745.
(53) Neyshtadt, S.; Jahnke, J. P.; Messinger, R. J.; Rawal, A.; Peretz, T. S.; Huppert, D.; Chmelka, B. F.; Frey, G. L. *J. Am. Chem. Soc.* **2011**, *133*, 10119.
(54) Corma, A. *Chem. Rev.* **1997**, *97*, 2373.
(55) Granja, L. P.; Martínez, E. D.; Troiani, H.; Sanchez, C.; Soler Illia, G. J. A. A. *ACS Appl. Mater. Interfaces* **2017**, *9*, 965.
(56) He, J.; Song, Z.; Ma, H.; Yang, L.; Guo, C. *J. Mater. Chem.* **2006**, *16*, 4307.
(57) Itoh, T.; Ishii, R.; Matsuura, S.; Mizuguchi, J.; Hamakawa, S.; Hanaoka, T.; Tsunoda, T.; Mizukami, F. *Colloids Surf., B* **2010**, *75*, 478.
(58) Oda, I.; Iwaki, M.; Fujita, D.; Tsutsui, Y.; Ishizaka, S.; Dewa, M.; Nango, M.; Kajino, T.; Fukushima, Y.; Itoh, S. *Langmuir* **2010**, *26*, 13399.
(59) Noji, T.; Kamidaki, C.; Kawakami, K.; Shen, J.-R.; Kajino, T.; Fukushima, Y.; Sekitoh, T.; Itoh, S. *Langmuir* **2011**, *27*, 705.
(60) Hussain, S.; Franck, J. M.; Han, S. *Angew. Chem., Int. Ed.* **2013**, *52*, 1953.
(61) Stone, K. M.; Voska, J.; Kinnebrew, M.; Pavlova, A.; Junk, M. J. N.; Han, S. *Biophys. J.* **2013**, *104*, 472.
(62) Reckel, S.; Gottstein, D.; Stehle, J.; Löhr, F.; Verhoefen, M.; Takeda, M.; Silvers, R.; Kainosho, M.; Glaubitz, C.; Wachtveitl, J.; Bernhard, F.; Schwalbe, H.; Güntert, P.; Dötsch, V. *Angew. Chem., Int. Ed.* **2011**, *50*, 11942.
(63) Berliner, L. J.; Grunwald, J.; Hankovszky, H. O.; Hideg, K. *Anal. Biochem.* **1982**, *119*, 450.
(64) Altenbach, C.; Flitsch, S. L.; Khorana, H. G.; Hubbell, W. L. *Biochemistry* **1989**, *28*, 7806.
(65) Höfer, P.; Grupp, A.; Nebenführ, H.; Mehring, M. *Chem. Phys. Lett.* **1986**, *132*, 279.
(66) Schweiger, A. *Angew. Chem., Int. Ed. Engl.* **1991**, *30*, 265.
(67) Yang, Q.; Zhou, Q.; Somasundaran, P. *Colloids Surf., A* **2007**, *305*, 22.
(68) Štangar, U. L.; Hüsing, N. *Silicon Chem.* **2003**, *2*, 157.
(69) Lakatos, M.; Lanyi, J. K.; Szakács, J.; Váró, G. *Biophys. J.* **2003**, *84*, 3252.
(70) Chemin, N.; Klotz, M.; Rouessac, V.; Ayral, A.; Barthel, E. *Thin Solid Films* **2006**, *495*, 210.
(71) Wahab, M. A.; He, C. *Langmuir* **2009**, *25*, 832.
(72) Auvray, X.; Petipas, C.; Anthore, R.; Rico-Lattes, I.; Lattes, A. *Langmuir* **1995**, *11*, 433.
(73) Zhao, D.; Feng, J.; Huo, Q.; Melosh, N.; Frederickson, G. H.; Chmelka, B. F.; Stucky, G. D. *Science* **1998**, *279*, 548.
(74) Sun, H.; Nathans, J. *J. Biol. Chem.* **2001**, *276*, 11766.
(75) Herz, J.; Verhoefen, M.-K.; Weber, I.; Bamann, C.; Glaubitz, C.; Wachtveitl, J. *Biochemistry* **2012**, *51*, 5589.
(76) Druckmann, S.; Ottolenghi, M. *Biophys. J.* **1981**, *33*, 263.
(77) Columbus, L.; Hubbell, W. L. *Trends Biochem. Sci.* **2002**, *27*, 288.
(78) Ježek, P.; Bauer, M.; Trommer, W. E. *FEBS Lett.* **1995**, *361*, 303.
(79) Butterfield, D. A.; Markesbery, W. R. *Neurosci. Lett.* **1983**, *35*, 221.
(80) Shi, L.; Ahmed, M. A. M.; Zhang, W.; Whited, G.; Brown, L. S.; Ladizhansky, V. *J. Mol. Biol.* **2009**, *386*, 1078.
(81) Andersson, M.; Malmerberg, E.; Westenhoff, S.; Katona, G.; Cammarata, M.; Wöhri, A. B.; Johansson, L. C.; Ewald, F.; Eklund, M.; Wulff, M.; Davidsson, J.; Neutze, R. *Structure* **2009**, *17*, 1265.
(82) Dioumaev, A. K.; Brown, L. S.; Shih, J.; Spudich, E. N.; Spudich, J. L.; Lanyi, J. K. *Biochemistry* **2002**, *41*, 5348.
(83) Váró, G.; Brown, L. S.; Lakatos, M.; Lanyi, J. K. *Biophys. J.* **2003**, *84*, 1202.
(84) Váró, G.; Lanyi, J. K. *Biochemistry* **1991**, *30*, 5016.
(85) Singer, S. J. *Annu. Rev. Biochem.* **1974**, *43*, 805.
(86) Hirota, S.; Hattori, Y.; Nagao, S.; Taketa, M.; Komori, H.; Kamikubo, H.; Wang, Z.; Takahashi, I.; Negi, S.; Sugiura, Y.; Kataoka, M.; Higuchi, Y. *Proc. Natl. Acad. Sci. U. S. A.* **2010**, *107*, 12854.
(87) Hüttemann, M.; Pecina, P.; Rainbolt, M.; Sanderson, T. H.; Kagan, V. E.; Samavati, L.; Doan, J. W.; Lee, I. *Mitochondrion* **2011**, *11*, 369.

DOI: 10.1021/jacs.7b06863
J. Am. Chem. Soc. 2018, 140, 3892−3906

(88) Lambeth, D. O.; Campbell, K. L.; Zand, R.; Palmer, G. *J. Biol. Chem.* **1973**, *248*, 8130.
(89) Kurihara, M.; Sano, S. *J. Biol. Chem.* **1970**, *245*, 4804.

DOI: 10.1021/jacs.7b06863
J. Am. Chem. Soc. 2018, 140, 3892−3906

Supporting Information

Functionally active membrane proteins incorporated in mesostructured silica films

Justin P. Jahnke,[1] Matthew N. Idso,[1] Sunyia Hussain,[1] Matthias J.N. Junk,[1] Julia M. Fisher,[1] David D. Phan,[1] Songi Han,[1,2] Bradley F. Chmelka[1]*

[1] Department of Chemical Engineering and [2] Department of Chemistry and Biochemistry, University of California, Santa Barbara, California, 93106 United States

* To whom correspondence should be addressed: bradc@engineering.ucsb.edu

Contents

1. Protocols for expressing, purifying, and spin-labeling proteorhodopsin (PR) for incorporation into mesostructured silica films

The green-absorbing PR gene (BAC31A8), with the three natural cysteines mutated to serines, also with the additional photocycle-slowing E108Q mutation, was provided in a pTrcHis2 vector by E.F. DeLong and G. Whited, Genencor. The triple-cysteine mutant (TCM) is the most commonly studied PR variant, because it is less subject to oxidation than the true wild-type protein, and therefore has enhanced stability[1] and only minor functional differences.[2] The PR TCM is denoted here as "wild-type." Both wild-type PR and PR E108Q genes were subsequently cloned into the ampicillin-resistant pET22b vector (Novagen) using standard molecular biology techniques, which enable the addition of a 6X Histidine tag at the C-terminal end of the protein which facilitates protein purification via nickel chromatography. The cysteine point mutations (A174C and T177C) made for subsequent EPR investigations were introduced by modifying the PR E108Q template by site-directed-mutagenesis methods, such as those provided by the Quikchange kit (Stratagene, La Jolla, California).

PR was expressed by transformation of the PR-pET26b vector (or desired cysteine mutant) into *E. coli* strain BL21(DE3) competent cells. Individual bacterial colonies or glycerol stocks derived from transformants were used to inoculate a 10 mL culture of LB media containing 100 μg/mL ampicillin and allowed to grow overnight at 37˚C. Liter-scale batches were then grown from this starter culture, and overexpression of PR was induced by the addition of 1 mM isopropropyl-β-D-thiogalactopyranoside (IPTG) and 10 μM all-trans-retinal upon reaching a cell density with OD_{600} ~ 0.8. The pink-colored PR-expressing cells were then harvested by centrifugation after 4 h of growth at 37 ˚C.

The remainder of the purification procedure was carried out in a cold environment (4 ˚C) in solutions that contained a phosphate buffer (50 mM potassium phosphate, 150 mM KCl, pH 8.2). The cells were first resuspended in phosphate buffered solution with 20 mM $MgCl_2$ and 0.2 mg/ml lysozyme, incubated with shaking for 1 h, and then lysed by sonication. After a low-speed centrifugation step to remove unbroken cells (2000 g), membranes containing PR were obtained by ultracentrifugation (220,000 g). Membrane proteins were then solubilized overnight in phosphate buffered solution containing 2 wt% of the dodecyl-β-D-maltoside (DDM) surfactant. The unsolubilized membrane portions were pelleted by high-speed centrifugation (15,000 g), and the amount of PR was quantified by UV-visible spectroscopy, as established in the literature.[3,4] The PR was then incubated with an appropriate amount of Ni-NTA agarose His-tag affinity resin (Qiagen, MD) equilibrated with phosphate buffered solution containing 0.05 wt% DDM. After binding the PR, the resin was washed with at least 10 resin volumes of phosphate buffered solution with 0.05 wt% DDM and 25 mM imidazole.

The spin-labeling procedure of PR mutants A174C and T177C was carried out while PR was bound to the Ni-NTA resin and in greater than 15 mL of the phosphate buffered solution with 0.05 wt% DDM titrated to pH 7. A 5X molar excess of the nitroxide label (1-oxyl-2,2,5,5-

tetramethyl-Δ3-pyrroline-3-methyl) methanethiosulfonate (MTSL, Toronto Research Chemicals) was added from a 340 mM DMSO stock solution of MTSL and allowed to react overnight at 4 ˚C. After labeling, the sample was washed with 10 resin volumes of phosphate buffered solution with 0.05% DDM and 25 mM imidazole to remove unreacted MTSL.

For both spin-labeled and unlabeled PR, elution of the protein from the Ni-NTA resin was carried by removing as much buffered solution as possible from the resin and incubating with an elution buffer containing 450 mM imidazole and 0.1 wt% of the PR monomer-enriching 1,2-diheptanoyl-*s*,*n*-glycero-3-phosphocholine (diC_7PC, Avanti Polar Lipids) surfactant. Surfactant-associated MTSL and imidazole were removed by filtration with Sephadex gel desalting columns (GE Healthcare) equilibrated with 0.1 wt% diC_7PC in the phosphate buffered solution. The PR solutions obtained were then concentrated to ~100 μL volumes using centrifugal concentrators (10,000 MWCO; Millipore). The sample volume was increased to ~2.2 mL with phosphate buffered solution containing 2 wt% diC_7PC and then the sample was mix overnight to increase the population of monomeric PR. Size-exclusion fast protein chromatography (FPLC) carried out the next day as described in the main text, using the standard DDM buffer (0.05 wt% DDM) to elute the protein.

2. Blue-Native PAGE gel of DDM-solubilized monomeric and oligomeric proteorhodopsin isolated by size exclusion chromatography

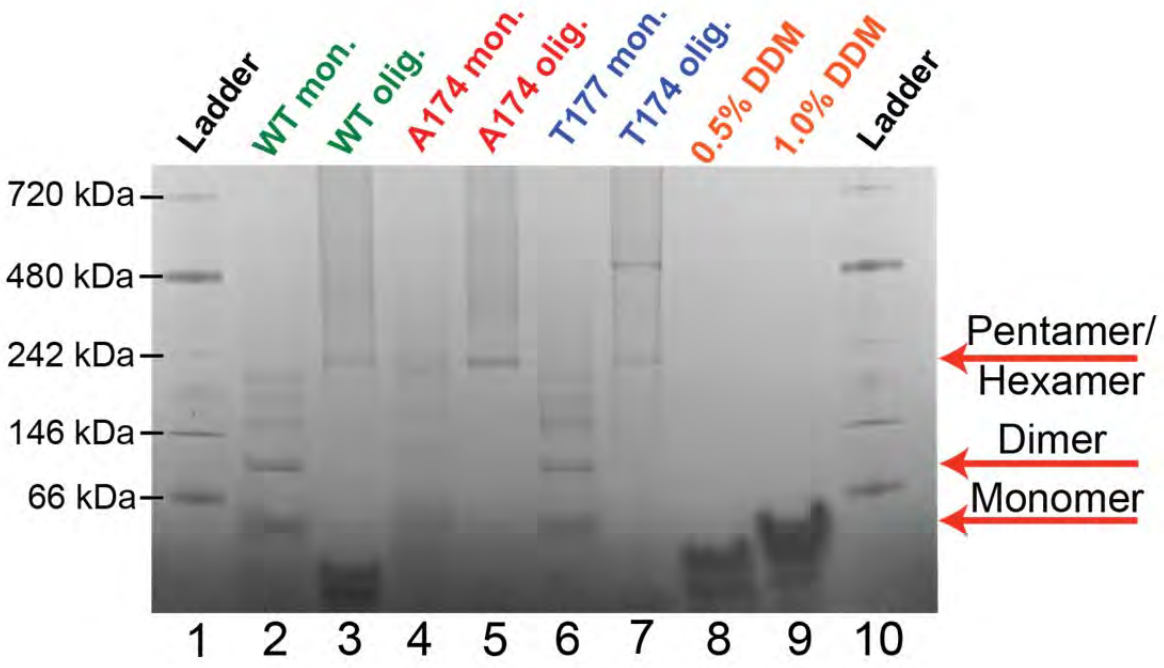

Figure S1. Blue-Native PAGE gel of wild-type (WT, well 2), A174R1-E108Q (well 4), and T177R1-E108Q (well 6) proteorhodopsin monomers isolated by size exclusion chromatography and exchanged non-buffered hydrochloric acid solutions (pH~4) with 0.05% DDM. Oligomeric proteorhodopsin in alkaline-buffered solutions (pH 9) collected from the same size-exclusion chromatography experiments are shown in wells 3, 5 and 7. The monomeric WT PR sample (well 2) show one intense band below the 66 kDa marker (well 1) and another below the 146 kDa marker (well 1) that are assignable to monomeric and dimeric proteorhodopsin species.[5] A number of lower intensity bands are observed above the 146 kDa marker (well 1) that presumably arise from oligomeric assemblies with more than two proteorhodopsin molecules. The wild-type proteorhodopsin oligomer sample (well 3) has a band at ~242 kDa that originates from pentameric/hexameric proteorhodopsin, while the two additional bands at molecular weights lower than that of monomeric proteorhodopsin likely arise from DDM micelles, as shown in wells 8 and 9. The monomeric and oligomeric fractions of both the spin-labeled A174R1-E108Q and T177R1-E108Q proteorhodopsin samples showed distributions similar to those of the wild-type proteins. Aqueous solutions (pH~7) with 0.5% and 1.0% DDM are shown in wells 8 and 9, respectively.

3. Images of DDM+diC$_7$PC-directed mesostructured silica films containing proteorhodopsin prepared with various compositions and synthesis conditions

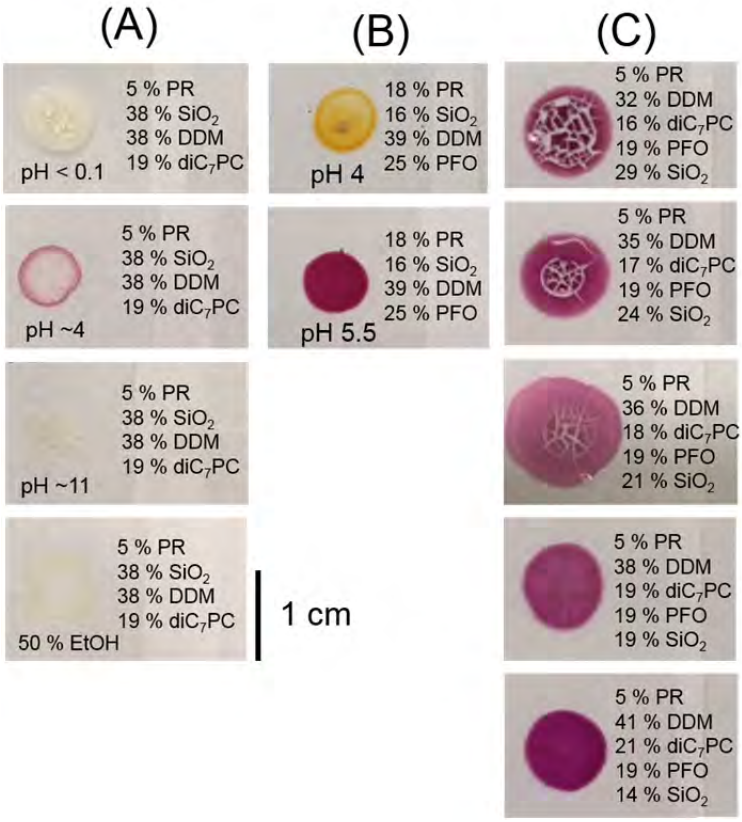

Figure S2. Macroscopic optical images of 50-100-μm-thick DDM+diC$_7$PC-directed silica films containing PR and cast on glass slides **(A)** without PFO under various pH and co-solvent conditions, **(B)** with PFO at either pH 4 or pH 5.5, and **(C)** using less water and with various silica contents. Mildly acidic (pH 4) synthesis conditions yielded films with purple colorations, consistent with functionally active PR. By comparison, films synthesized under conditions typical of conventional mesostructured silica materials, including at high acidities (pH <0.1), highly alkalinities (pH 11) or with 50% ethanol co-solvent, appeared yellow or transparent, indicative of denatured PR. As shown in (B), the anionic surfactant PFO promotes the formation of films with more homogeneous distributions of PR, though pH conditions higher than pH 4, such as at pH 5.5, are required to obtain films with functionally active PR. As the pI of PR is pH 5.8, PR is positively charged at pH 4 and therefore likely denatures in the presence of PFO as a result of strong attractive electrostatic interactions between PFO and PR, which are weaker at higher pH conditions. The macroscopic images in (C) reveal a lower propensity for macroscopic crack formation in silica films as SiO_2 content is decreased from 29 wt% to 14 wt%, which can be reduced by slowing the rate of drying.

4. N_2 sorption isotherm and BJH pore-distribution for DDM+diC_7PC-directed silica

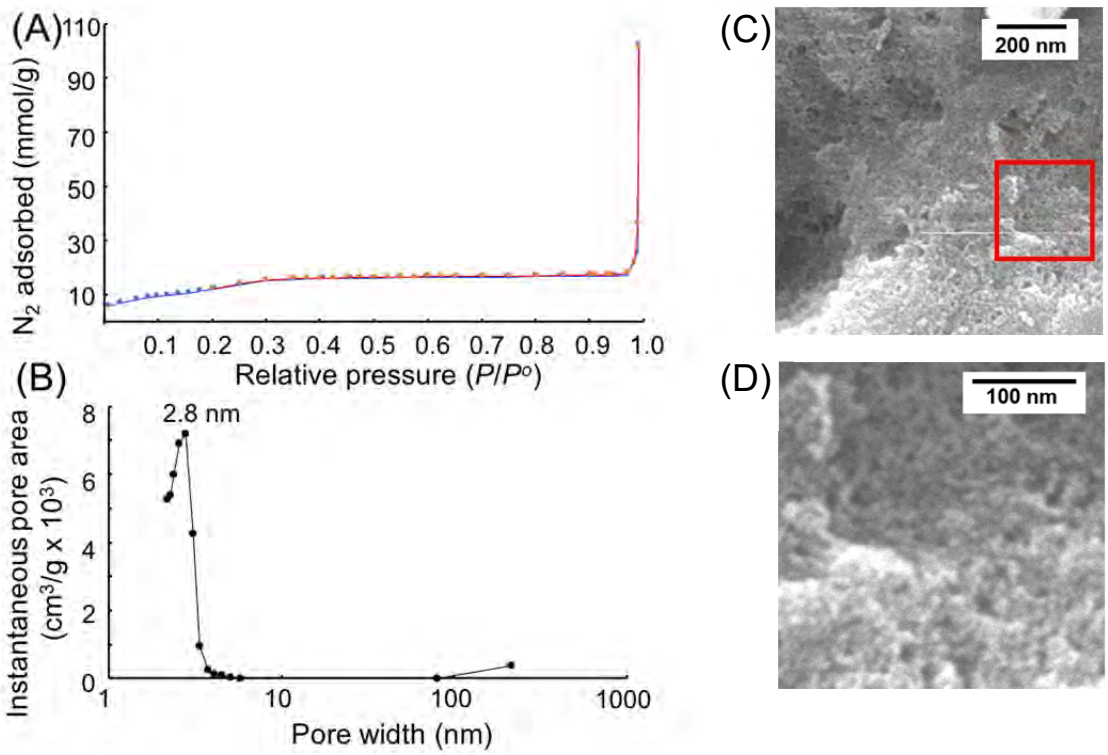

Figure S3. (A) N_2 adsorption (blue) and desorption (red) isotherms acquired from calcined DDM+diC_7PC-directed mesostructured silica materials synthesized with 40 wt% DDM, 20 wt% diC_7PC and 40 wt% SiO_2. The N_2 isotherm appears similar to a Type IV isotherm, but with a small hysteresis that indicates reversible capillary condensation and a substantial increase in N_2 adsorbed at the highest relative pressure. **(B)** Pore-size distribution calculated from the adsorption isotherm by using the BJH method, which exhibits a maximum ~2.8 nm, and a relatively narrow full-width-half maximum of 1 nm. This indicates a contraction of the framework as a result of calcination, with retention of relatively uniform mesopore dimensions. **(C, D)** Scanning electron microscopy images show a distribution of nanoscale textural features that are consistent with the BJH pore-size distribution and the small-angle X-ray scattering analyses for the as-synthesized material in Figure 2A.

5. Small-angle X-ray scattering patterns of mesostructured silica materials without and with proteorhodopsin guest species

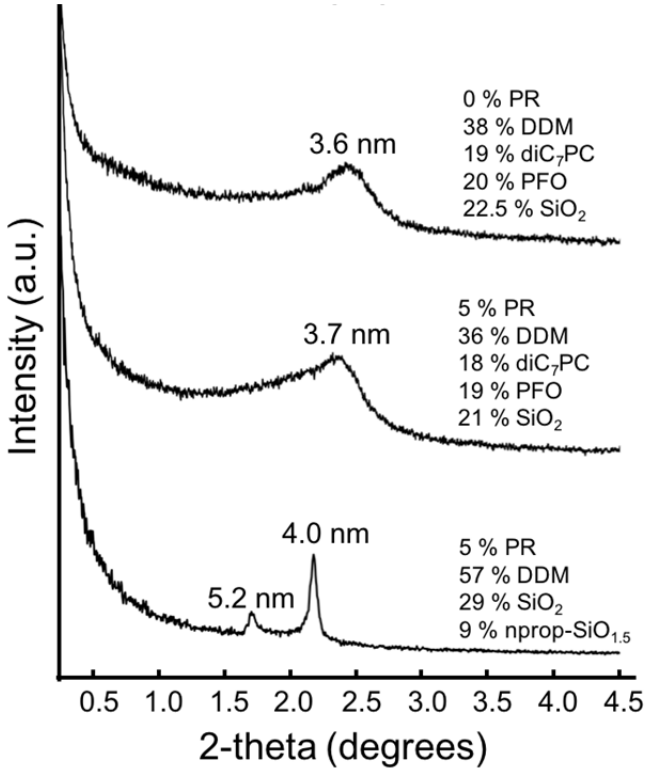

Figure S4. (A) Small-angle X-ray scattering (SAXS) patterns of mesostructured silica materials synthesized with various surfactant compositions: (**top**) 0 wt% PR, (**middle**) 5 wt% PR and (**bottom**) 5 wt% PR with low H_2O content during synthesis (H_2O ratio of 3.5:15), 29 wt% of SiO_2, and 9 wt% of *n*-propyl-$SiO_{1.5}$ organosilica.

6. Small-angle X-ray scattering patterns of DDM+diC$_7$PC-directed mesostructured silicas with different compositions of DDM and diC$_7$PC surfactants or calcined without PR

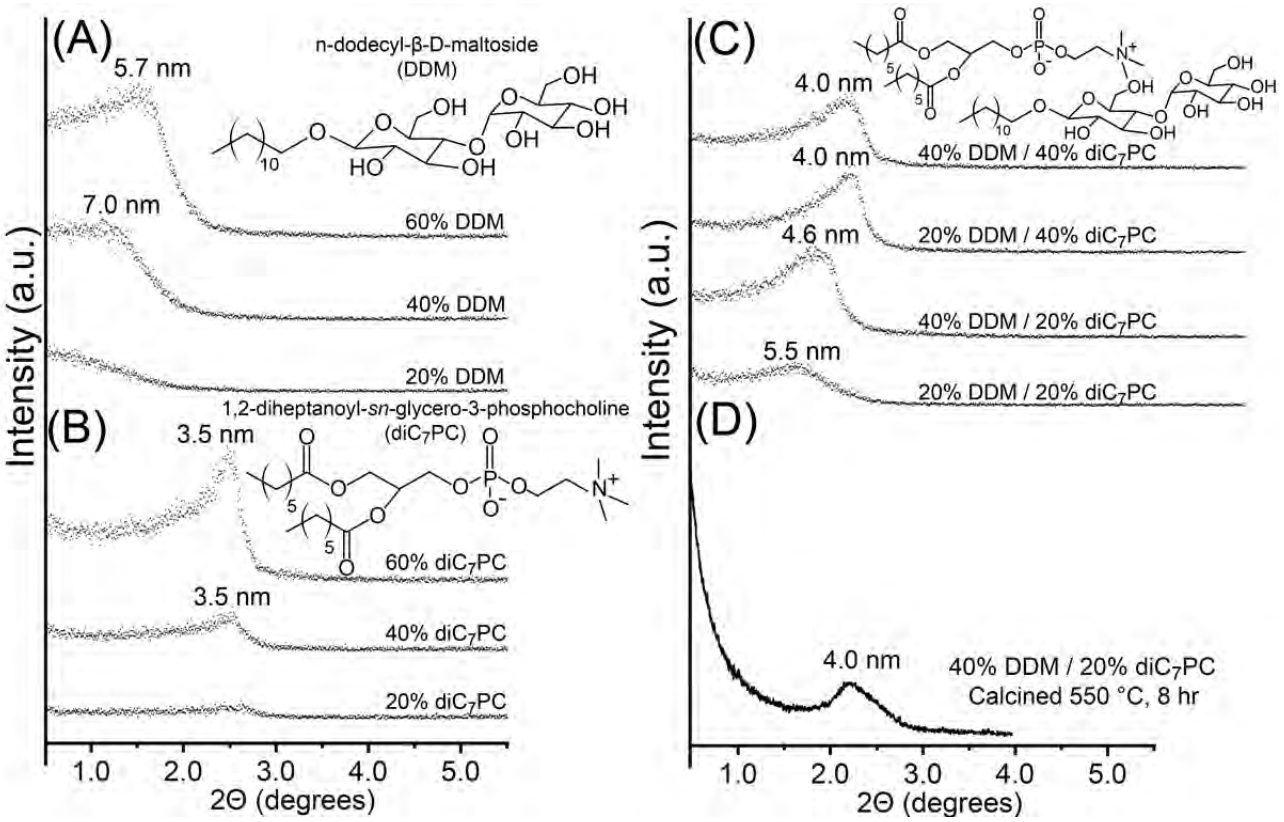

Figure S5. Small-angle X-ray scattering (SAXS) patterns of mesostructured silica materials synthesized using various quantities of **(A)** *n*-dodecyl-β-D-maltoside (DDM), **(B)** 1,2-diheptanoyl-*sn*-glycero-3-phosphocholine (diC$_7$PC), and **(C)** mixtures of DDM and diC$_7$PC as structure-directing surfactant species. Surfactant quantities are expressed as mass percentages of the final material (silica accounts for the balance), assuming complete solvent removal and silica cross-linking. Material precursor solutions were prepared by adding appropriate quantities of DDM and/or diC$_7$PC surfactants to aqueous solutions containing tetraethoxysilane silica precursor species, stirred under acidic conditions for 1.5 h. After the surfactants were dissolved, material solutions were titrated to pH 3-4 using 40 mM NaOH (aq.) and cast into Petri dishes under ambient conditions and allowed to dry for 2 days before SAXS characterization. **(D)** SAXS pattern of calcined mesostructured silica synthesized with 40% DDM, 20 % diC$_7$PC and 40% SiO_2, as described above, then calcined at 550 °C for 8 h; a single broad reflection is present at a *d*-spacing of 4.0 nm, consistent with contraction that occurs as a result of calcination of the as-synthesized material (*d*-spacing 4.6 nm, part C, 40% DDM and 20% diC$_7$PC).

7. Small-angle X-ray scattering patterns of DDM+diC_7PC-directed mesostructured silica with different loadings of proteorhodopsin (PR) species and PFO surfactants

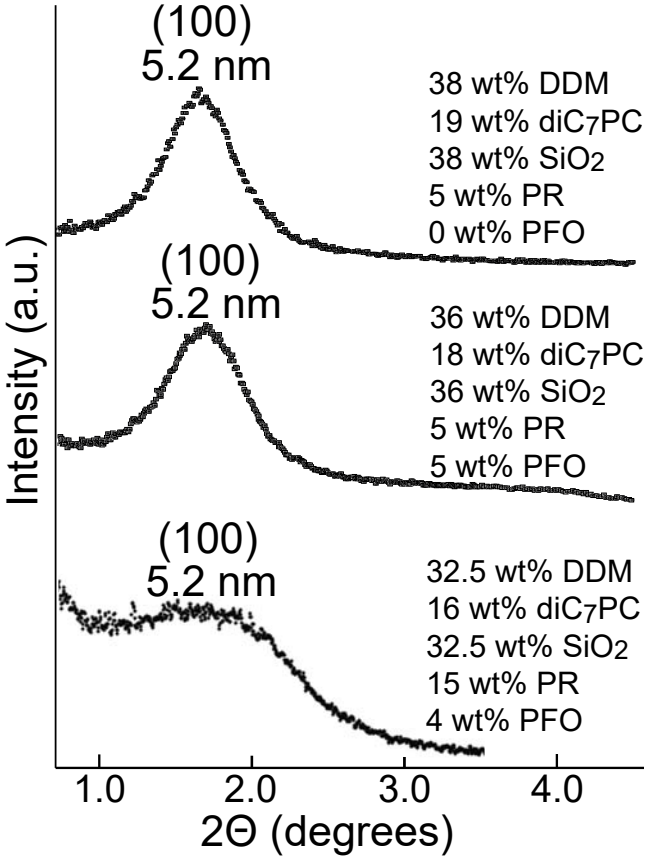

Figure S6. Small-angle X-ray scattering (SAXS) patterns of 50-μm thick DDM- and diC_7PC-directed mesostructured silica films with 5 wt% PR without (**top**) and with (**middle**) 5 wt% of PFO. The film that incorporates 5 wt% of PFO yields a primary *(100)* SAXS reflection at 1.7 ^{o} that is slightly broadened, yet otherwise identical to those of films without PFO, establishing the minor local effects of PFO molecules on the co-assembly interactions during formation of the silica-surfactant mesostructure. The SAXS reflection pattern (**bottom**) of a film that incorporates 15 wt% of PR has a primary *(100)* reflection position shifted to 1.7^{o}, corresponding to a 5.2 nm *d*-spacing, with a full-width-half-maximum of ~1.0 ^{o}.

8. Small-angle X-ray scattering patterns of P123-directed silica without and with DDM and 0.5 wt% proteorhodopsin

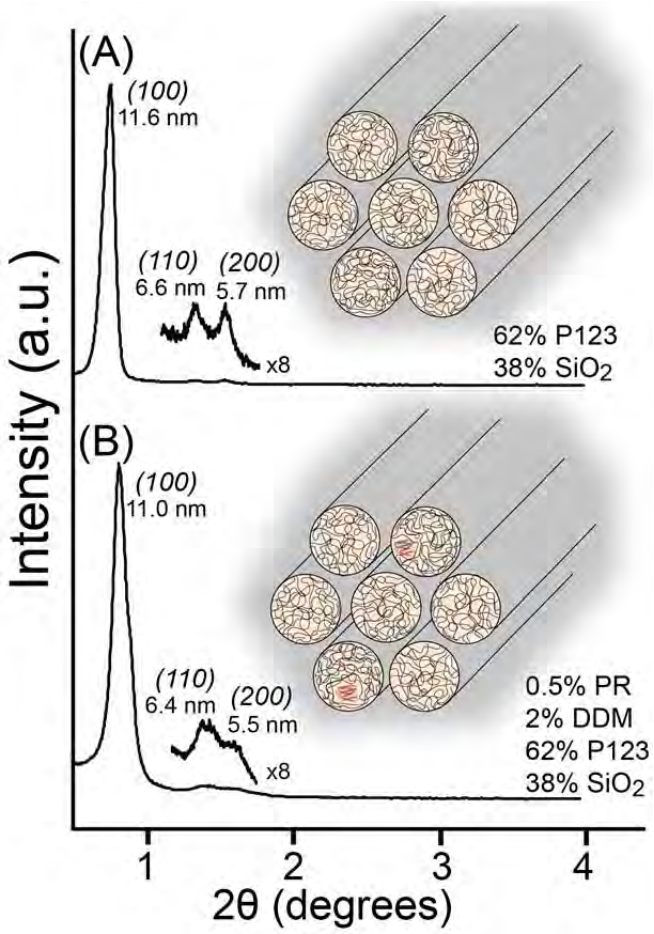

Figure S7. Small-angle X-ray scattering (SAXS) patterns from powders of P123-directed silica films **(A)** without and **(B)** with 0.5 wt% proteorhodopsin incorporated. Each pattern shows three reflections at ~0.8°, 1.3°, and 1.5° that are indexable to the (*100*), (*110*) and (*200*) reflections, respectively, associated with hexagonal (*p6mm)* mesostructural order. The patterns are similar, though with broader reflections observed in (B) for the film containing dilute PR and DDM, indicating reduced mesostructural order that diminishes further at higher PR loadings (not shown) and is accompanied by eventual loss of transparency of the films. Compared to conventional syntheses of P123-directed mesostructured silica, the somewhat lower extents of mesostructural ordering in these materials likely arises from the use of higher water contents, small quantities of DDM, and mild acidic conditions (pH ~4), which are necessary to stabilize PR molecules during co-assembly.

9. Table S1: Mechanical properties of mesostructured silica materials with 5 wt% PR

	Sample A		Sample B	
Region #	Hardness (MPa)	Modulus (MPa)	Hardness (MPa)	Modulus (MPa)
1	3.4	184	4.3	193
2	3.6	154	6.3	273
3	10.6	630	3.9	226
4	6.8	306	5.8	261
5	6.9	325	6.0	274
6	11.2	588	4.2	287
7	3.7	210	4.8	271
8	3.3	216	4.6	273
9	7.1	420	---	---
10	11.7	989	---	---
11	6.8	439	---	---
Average	6.8	406	5.0	257
St. deviation	3.0	239	0.9	29

Nano-indentation measurements were conducted to determine the hardness and modulus values of DDM+diC_7PC-directed mesostructured silica membranes containing 5 wt% proteorhodopsin guest species, without (Sample A) or with PFO (Sample B) synthesized on glass cover slips. The values for hardness and modulus reported in Table S1 were obtained using the Oliver-Parr method (which allowed for continuous measurement of hardness and modulus during loading) and represent the average hardness or modulus values obtained over the last 10% of the displacement. For each sample, several nano-indentation measurements were performed on different regions of the mesostructured silica membrane. Variations in the hardness and modulus values likely arise from heterogeneities in sample morphology and are more pronounced for Sample A, which exhibited a minor coffee-ring-like effect compared to Sample B, which was of more homogeneous. The composition of Sample A was 5 wt% PR, 38 wt% DDM, 19 wt% diC_7PC, 38 wt% SiO_2 and that of Sample B was 5 wt% PR, 36 wt% DDM, 18 wt% diC_7PC, 19 wt% PFO, 21 wt% SiO_2. These correspond to the materials for which SAXS and optical image results are presented in Figure 2B and 2C of the main manuscript.

10. Macroscopic images of cross-sections from mesostructured silica films with 5 wt% PR

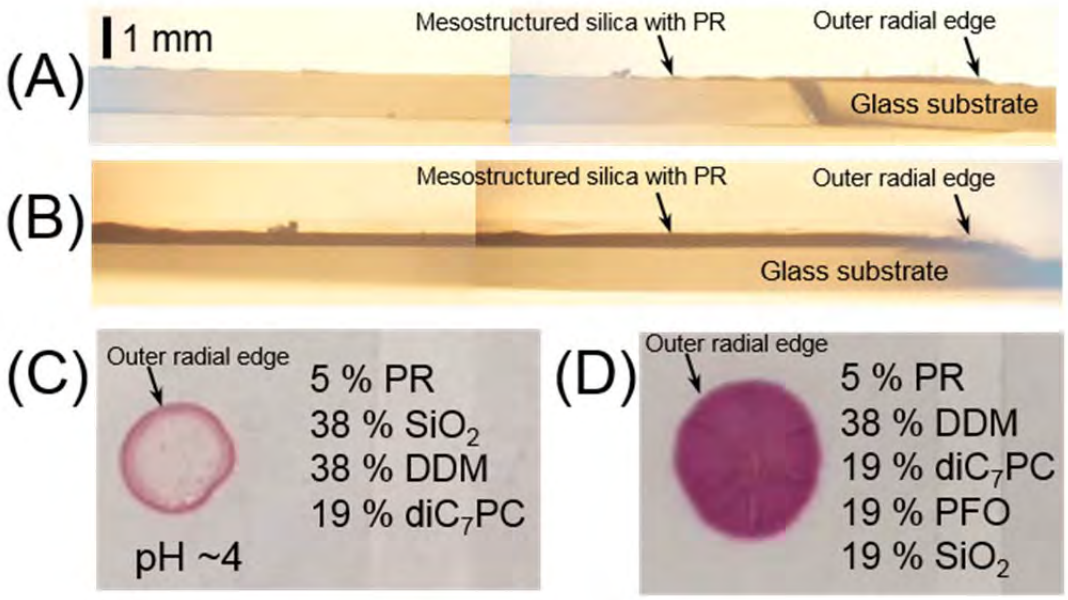

Figure S8. Macroscopic optical images of cross-sections from DDM+diC_7PC-directed mesostructured silica films synthesized with 5 wt% PR synthesized **(A)** without and **(B)** with 19 wt% PFO on glass substrates. The image in (A) was taken from **(C)** a film synthesized at pH 4 without PFO, which exhibits coffee-ring-like effects with the outer radial edge being thicker and darker than the center of the film. The image in (B) was taken from **(D)** a film with 19 wt% PFO, which yields a more homogeneous distribution of PR and thickness across the diameter of the film.

11. UV-visible absorption spectra of 20 wt% PFO mesostructured silica materials with and without PR

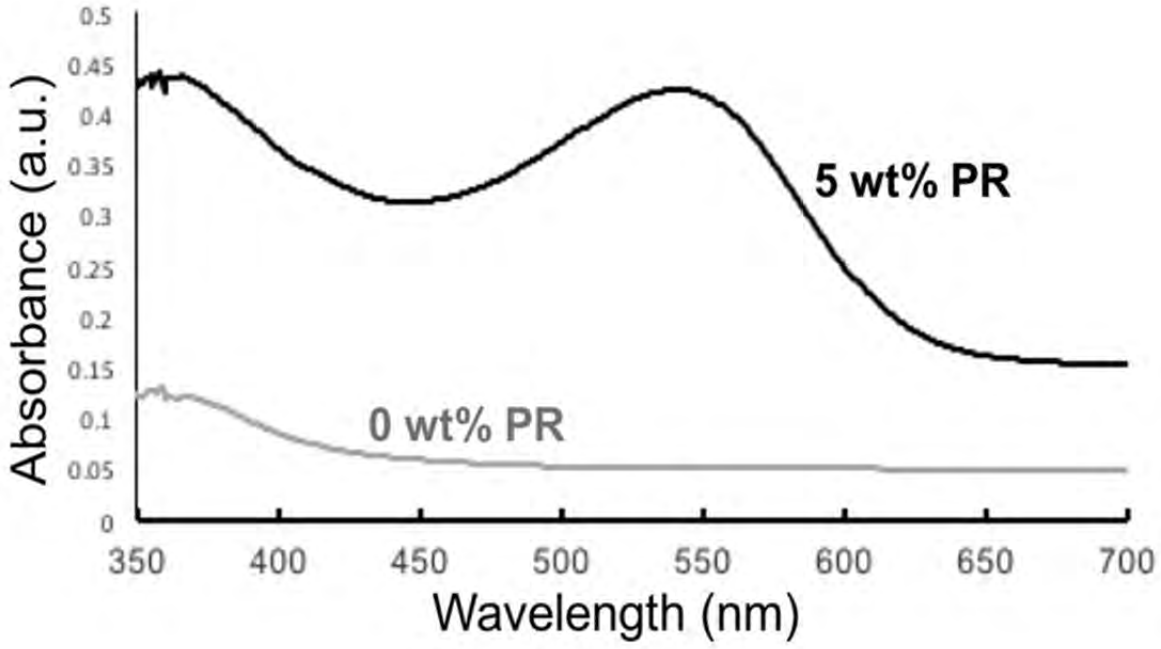

Figure S9. UV-visible absorption spectra acquired from DDM-diC_7PC+PFO-directed mesostructured silica films with either 0 wt% (grey) or 5 wt% (black) PR. The spectrum of materials without PR (grey) exhibits nearly constant and negligible absorbance over the visible range between 500 and 700 nm over which PR guests absorb. As neither film contains molecules that absorb at 700 nm, the greater absorption at 700 nm of films with PR (black) versus those without (grey) PR probably arises from differences in film thickness, morphology and/or alignment with incident light, rather than increased light scattering. The small absorbance centered at ~360 nm of films without PR (grey) likely originates from PFO molecules. The films were cast on borosilicate glass for both UV-visible absorption spectra shown here. These results indicate that the baseline background contribution can be considered to be minor in the absorbance spectrum for the otherwise identical DDM+diC_7PC+PFO-directed silica film containing 5 wt% PR.

12. Full 2D HYSCORE EPR spectrum of DDM-diC$_7$PC-directed mesostructured silica films containing 5 wt% PR

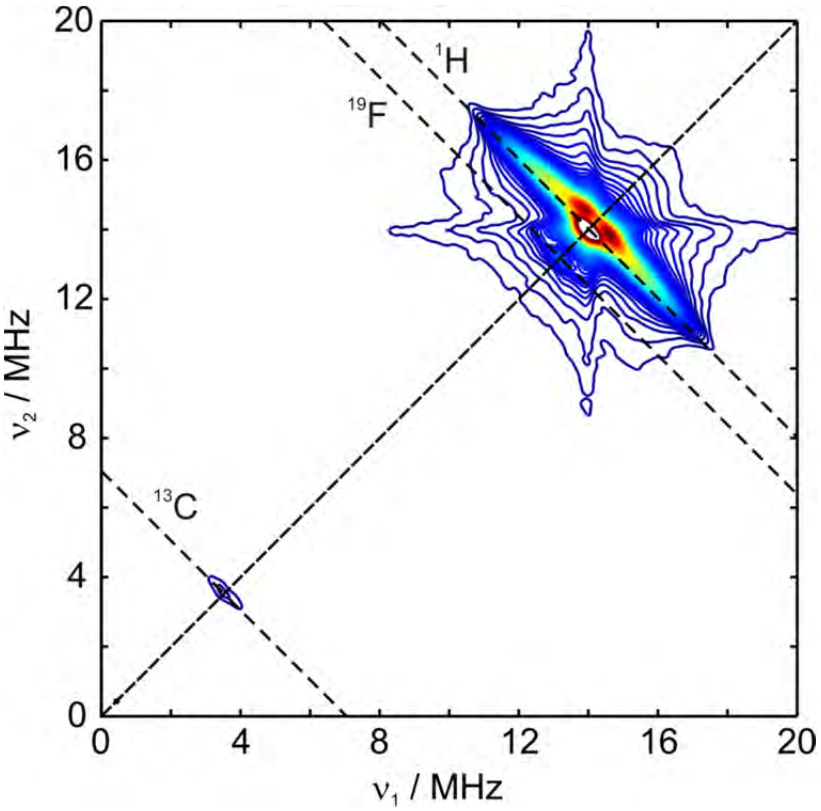

Figure S10. Full (+,+) quadrant of the HYSCORE EPR spectrum of a DDM+diC$_7$PC+PFO-directed silica film with 5 wt% proteorhodopsin labeled at the E-F loop residue 174 with the nitroxide spin label R1. The cumulative spectrum was obtained from two experiments recorded at 50 K with interpulse delays of 148 ns and 180 ns. Dashed anti-diagonals, which intersect the diagonal at 3.53 MHz, 13.19 MHz, and 14.02 MHz and correspond to the ^{13}C, ^{19}F, and ^{1}H Larmor frequencies at a magnetic field of 0.329 T, serve as guides to the eye. The lower cut-off value was decreased from 6% to 1.5% of the maximum signal intensity compared to the spectrum shown in Figure 4 of the main text. No appreciable signal intensity is observed in the (–,+) quadrant of the spectrum, which features signatures from strongly coupled nuclei with hyperfine couplings greater than their respective nuclear Larmor frequencies. Weak signal intensity at the ^{13}C Larmor frequency near the diagonal indicates weak coupling of the nitroxide spin to ^{13}C spins, which are present with a natural abundance of 1.1% in the protein and the surfactant.

13. $^{1}H\{^{19}F\}$ REDOR NMR spectrum of DDM+diC$_7$PC+PFO-directed mesostructured silica

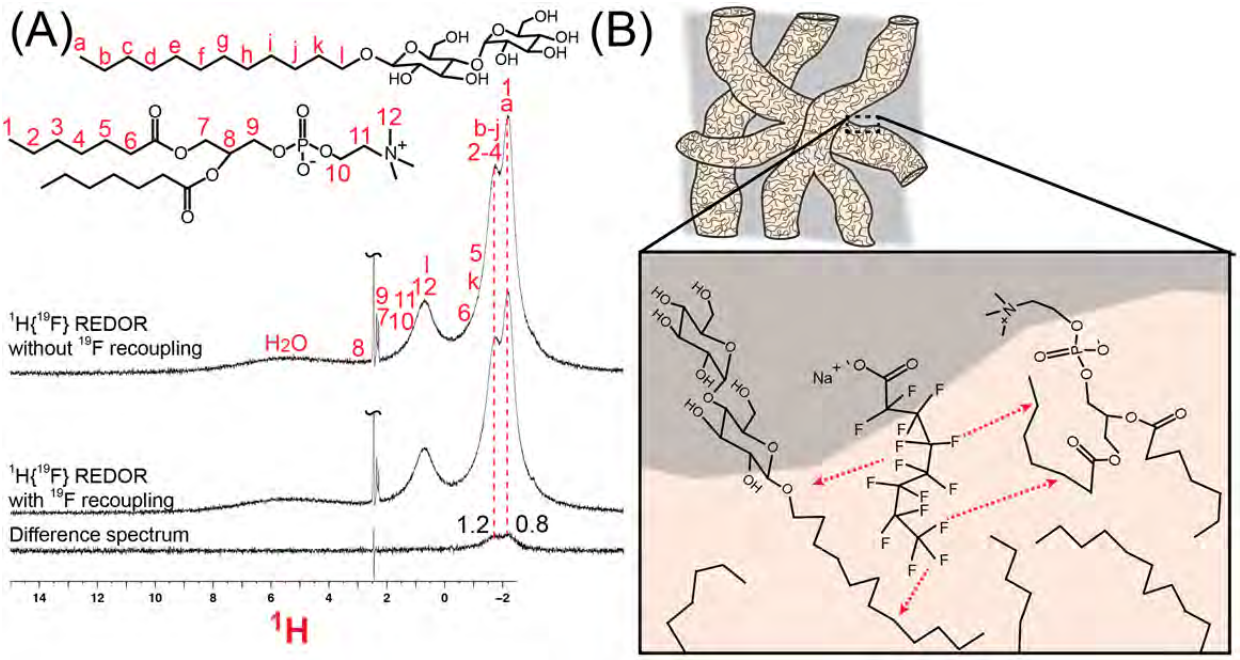

Figure S11. Solid-state $^{1}H\{^{19}F\}$ REDOR NMR spectra of DDM+diC$_7$PC+PFO-directed silica (5 wt% PFO), acquired without (**A, top**) and with (**A, middle**) reintroduction of ^{19}F-^{1}H dipolar couplings during a recoupling time of 0.11 ms, along with the corresponding difference spectrum (**A, bottom**). Signal intensities observed at 0.8 and 1.2 ppm (dotted red lines) are assignable to -CH_3 moieties *a* and *1* and -CH_2- moieties *b-j* and *2-4*, respectively, of the DDM and diC$_7$PC surfactant tails. As the only ^{19}F species in this material are associated with the PFO surfactant species, these signals establish the close proximities (<2 nm) of the PFO molecules to the structure-directing DDM and/or diC$_7$PC surfactants, as depicted schematically in (**B**). All spectra were acquired at MAS conditions of 15 kHz at approximately -20 °C.

14. Continuous-wave EPR spectra of P123-directed mesostructured silica materials containing PR with nitroxide spin labels at residues A174R1 or PR-T177R1

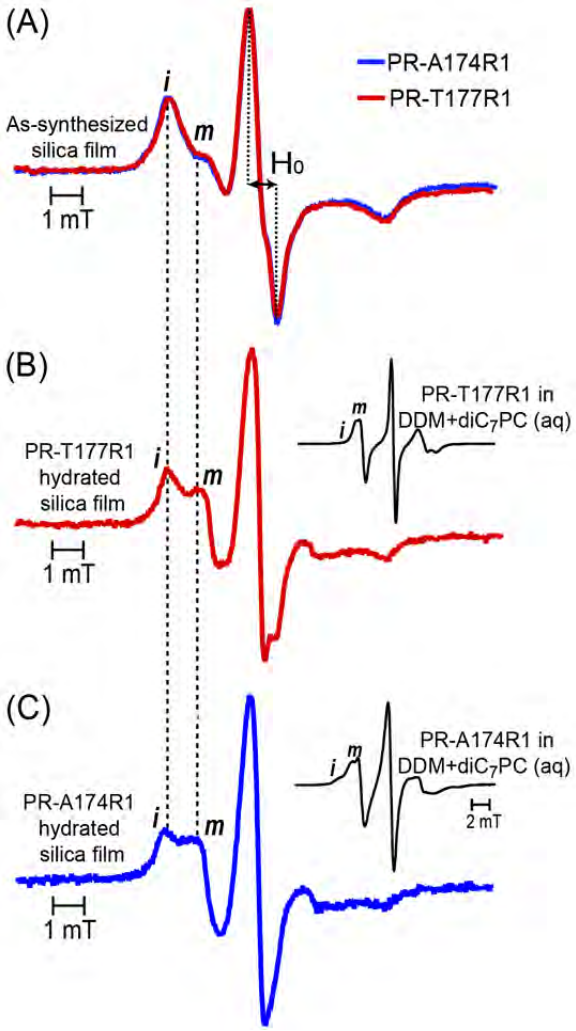

Figure S12. Continuous-wave EPR spectra of powders of P123-directed mesostructured silica films containing 0.5 wt% proteorhodopsin with nitroxide spin-labels at residues A174R1 or T177R1: **(A)** overlain spectra acquired from as-synthesized films, **(B,C)** spectra of films containing either (B) PR-T177R1 or (C) PR-A174R1 hydrated in alkaline-buffer (50 mM potassium phosphate, with 150 mM KCl, pH 9). The insets of (B) and (C) show the EPR spectra of the corresponding spin-labeled proteorhodopsin in alkaline-buffered DDM+diC$_7$PC micellar solutions under the same pH and buffer conditions. The as-synthesized P123-directed mesostructured materials with PR-A174R1 and PR-T177R1 have linewidths of 0.63-0.68 mT that are broader than the 0.23-0.31 mT linewidths of identically-labeled PR (Figure S6 B,C, insets) in alkaline-buffered DDM+diC$_7$PC micellar solutions. After hydrating the P123-directed mesostructured silicas in alkaline-buffered solutions, the EPR linewidths decrease by factors of 1.8 and 3.0 for materials that incorporate PR-A174R1 and PR-T177R1, respectively.

15. UV-visible absorption analyses of PR guest leaching from DDM+diC$_7$PC-silica materials upon exposure to alkaline buffered solutions

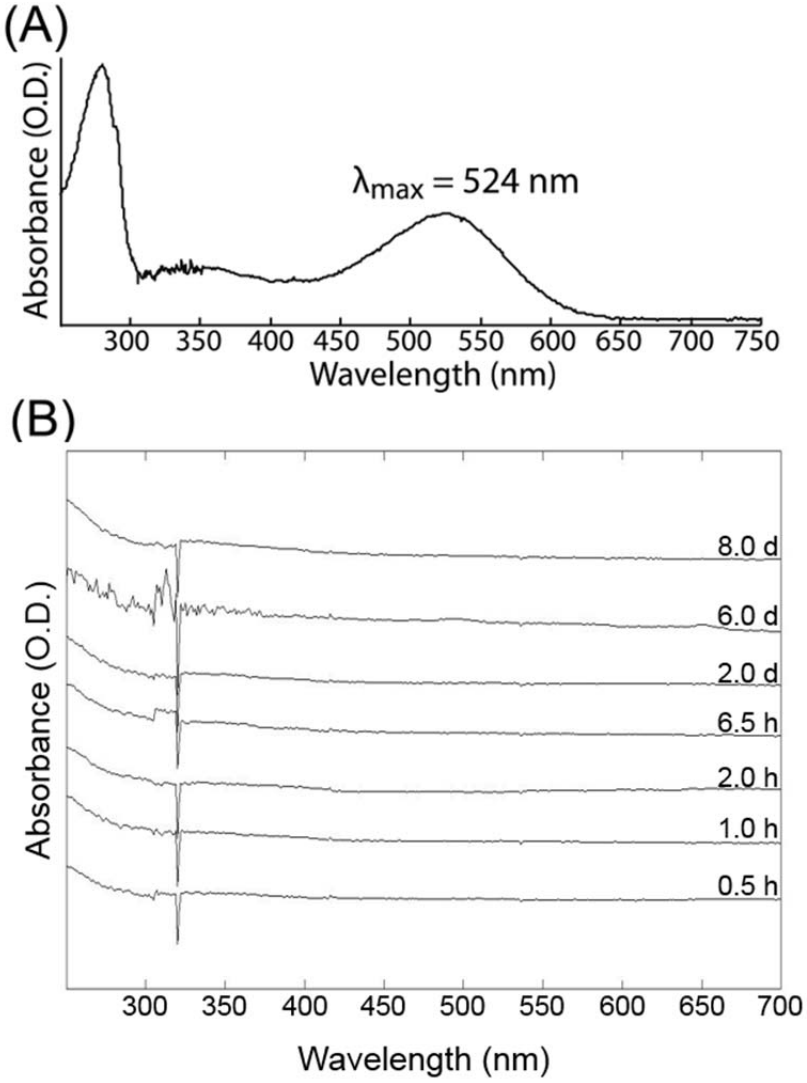

Figure S13. (A) Absorbance spectrum of PR in DDM micellar solutions under alkaline (pH~8.0) conditions. Two absorbance maxima are observed, one at 280 nm and another at 520 nm that arise largely from aromatic groups of the protein backbone and the retinal chromophore, respectively. **(B)** Absorbance of alkaline buffered solution with 0.5 wt% DDM that was mixed with DDM+diC$_7$PC-directed mesostructured silica materials that included 5 wt% wild-type PR at various amounts of times ranging from 0.5 h to 8 days from the initial exposure. No absorbance intensity is observed in the visible region near 520 nm or at 280 nm at any time, establishing that PR guests have not leached from the mesostructured silica materials. The positive absorbance at wavelengths below 300 nm may originate from scattering from in the sample or absorbance by the cuvette. Absorbance measurements in (B) were recorded on the supernatant solution obtained by centrifuging the material and solution mixture. The composition of mesostructured silica materials characterized in (B) was 28 wt% SiO_2, 60 wt% DDM, 7 wt% diC$_7$PC, and 5 wt% PR. Exposure of mesostructured silica materials with 16 wt% (or less) SiO_2 to aqueous solutions, however, resulted in partial leaching of PR guest species from the host materials.

16. Optical absorption difference spectra of 5 wt% PR (mutant E108Q) in an as-synthesized DDM+diC$_7$PC-directed mesostructured silica film and in *E. coli* membranes

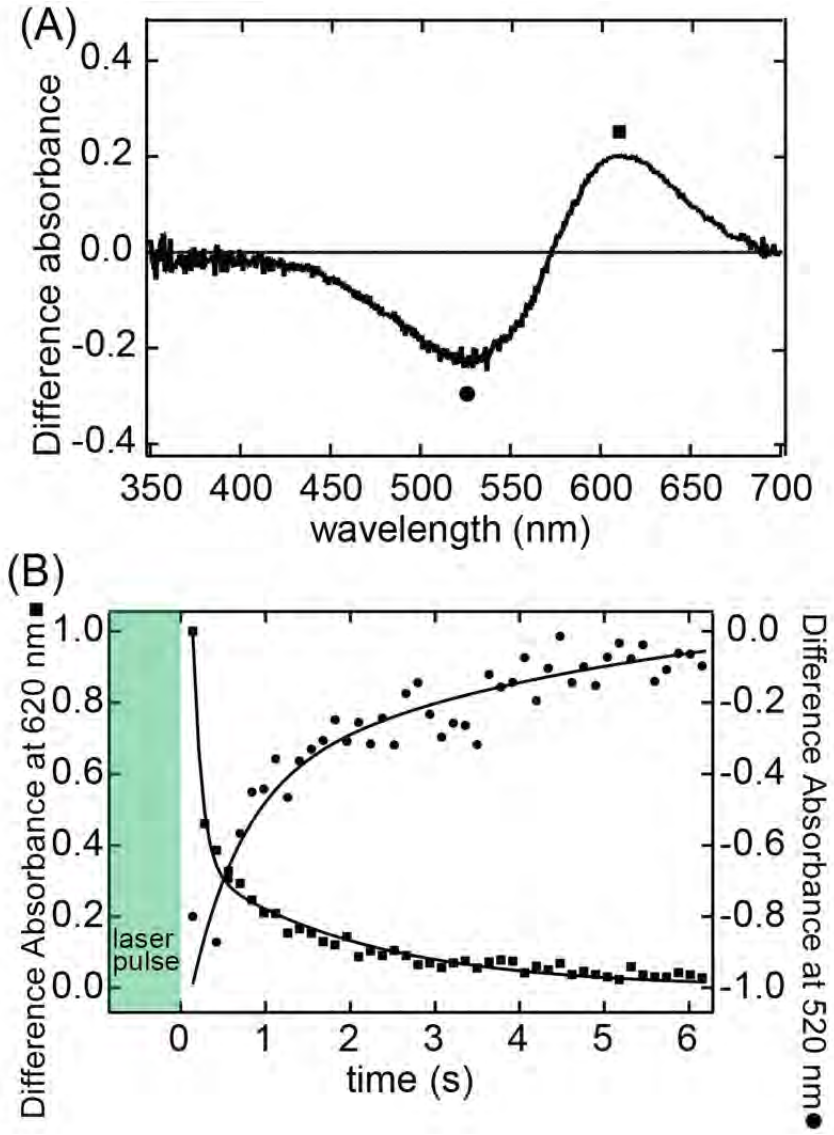

Figure S14. (A) Optical absorption difference spectra upon photo-activation of PR (slowed-photocycle E108Q mutant) spin-labeled with the nitroxide R1 at residue A174, incorporated at ~5 wt% in a DDM+diC$_7$PC-directed mesostructured silica film. The free-standing film was measured as-synthesized, without hydration or alkaline buffering. The spectrum shown was taken 130 ms after the sample was photo-activated with a 500 ms (~5 mW) green laser pulse. **(B)** Transient decay of the absorption amplitude at 620 nm (possibly a photo-intermediate in the later part of the PR photocycle stabilized by the DDM+diC$_7$PC-silica film), and intensity buildup at 520 nm (replenishment of the equilibrium PR state), are fit to biexponential curves.

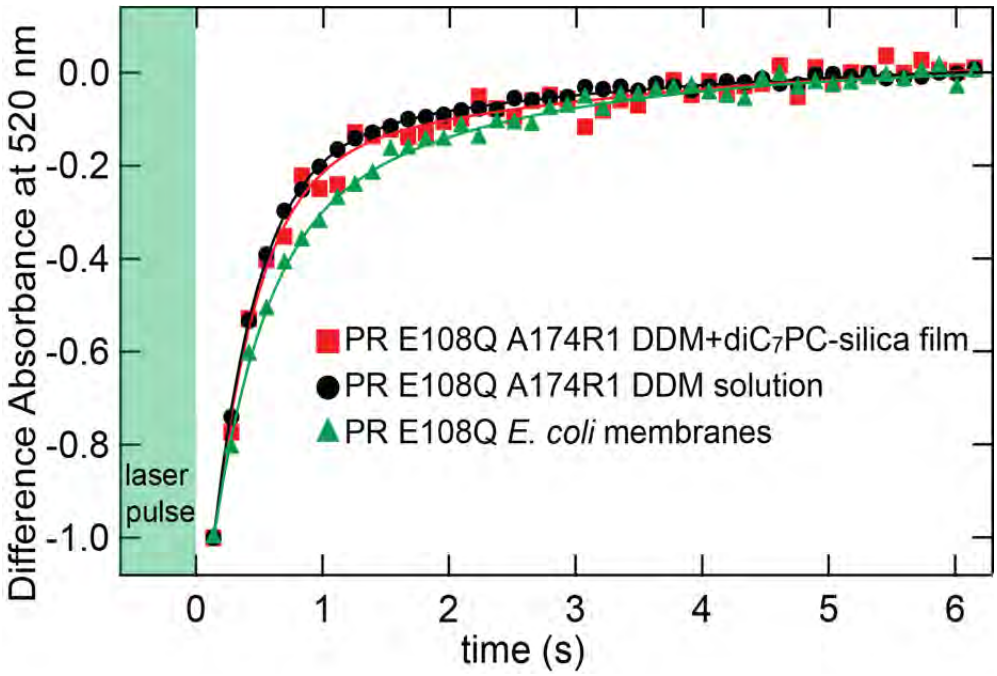

Figure S15. Time-resolved difference absorbance at 520 nm, following a green laser pulse, for PR in various environments: (1) in a DDM-diC_7PC-silica film hydrated with phosphate buffer (50 mM potassium phosphate, 150 mM KCl), (2) in a DDM micelle solution (0.05 wt% DDM in the same phosphate buffer), both shown in main text Figure 5, and (3) in extracted *E. coli* membranes resuspended in the phosphate buffer. All spectra were measured for mild alkaline conditions (pH 9) and fit to biexponential curves, which reveal that the PR E108Q photocycle displays similar characteristic time constants for the conditions tested. The increase in difference absorbance at 520 nm corresponds to the replenishment of the equilibrium *PR* state.

17. Continuous-wave EPR spectra of PR-A174R1 in DDM micellar solutions and P123-directed mesostructured silica with and without photo-activation

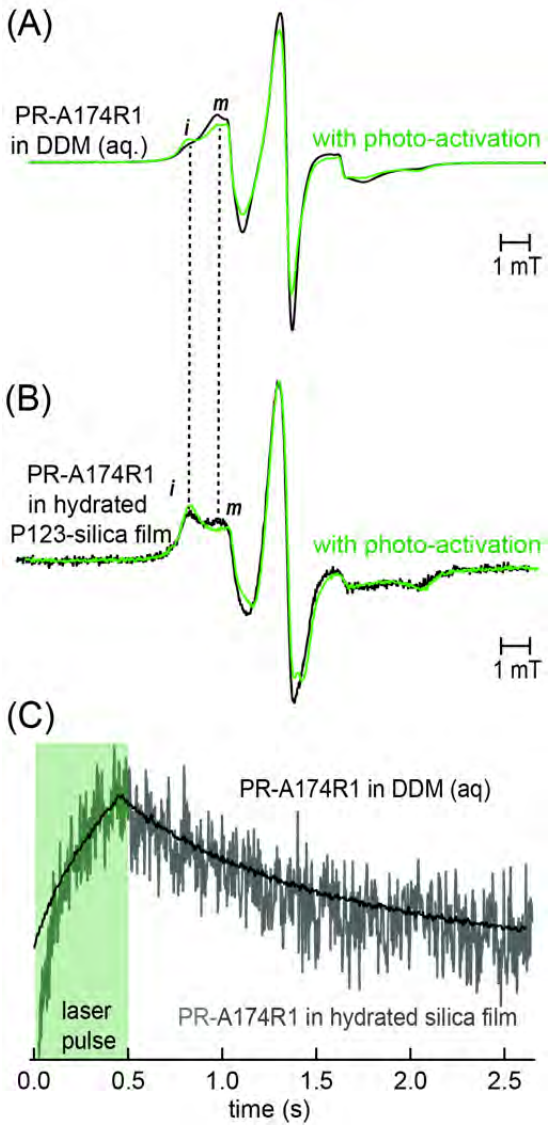

Figure S16. Continuous-wave EPR spectra (green) acquired under steady illumination by a green (532 nm) laser of the nitroxide spin-label (R1) attached to residue A174R1 of proteorhodopsin in **(A)** an alkaline (pH 9) buffered micellar solution (50 mM potassium phosphate, 150 mM KCl) of 0.05 wt% DDM and **(B)** a free-standing P123-directed mesostructured silica film with 0.5 wt% PR hydrated under the same buffer conditions. The EPR spectra (black lines) were acquired under identical conditions for the same samples without photo-activation for comparison. **(C)** Transient EPR amplitudes at the frequency corresponding to the relatively immobile (*i*) component of the EPR spectra of PR-A174R1 in hydrated P123-directed mesostructured silica films (grey line) and in the alkaline-buffered (pH 9) DDM+diC_7PC micellar solution (black line), directly following illumination of these samples with a green laser (~5 mW) pulse for 500 ms.

18. Supporting References

(1) Dioumaev, A. K.; Wang, J. M.; Bálint, Z.; Váró, G.; Lanyi, J. K. *Biochemistry* **2003**, *42*, 6582.

(2) Krebs, R. A.; Alexiev, U.; Partha, R.; DeVita, A. M.; Braiman, M. S. *BMC Physiol.* **2002**, *2*, 1.

(3) Lenz, M. O.; Huber, R.; Schmidt, B.; Gilch, P.; Kalmbach, R.; Engelhard, M.; Wachtveitl, J. *Biophys. J.* **2006**, *91*, 255.

(4) Friedrich, T.; Geibel, S.; Kalmbach, R.; Chizhov, I.; Ataka, K.; Heberle, J.; Engelhard, M.; Bamberg, E. *J. Mol. Biol.* **2002**, *321*, 821.

(5) Maciejko, J.; Mehler, M.; Kaur, J.; Lieblein, T.; Morgner, N.; Ouari, O.; Tordo, P.; Becker-Baldus, J.; Glaubitz, C. *J. Am. Chem. Soc.* **2015**, *137*, 9032.